CARBON FLUX AND PARTICLE-ASSOCIATED MICROBIAL REMINERALIZATION RATES IN THE NORTHERN BERING AND SOUTHERN CHUKCHI SEAS

By

Stephanie Hicks O'Daly, B.S.

A Thesis Submitted in Partial Fulfillment of the Requirements for the Degree of Master of Science

in

Chemical Oceanography

College of Fisheries and Ocean Sciences

University of Alaska Fairbanks

December 2019

APPROVED:

Dr. Andrew M.P. McDonnell, Committee Chair

Dr. Sarah M. Hardy, Committee Member

Dr. Mark A. Johnson, Committee Member

Dr. Russell R. Hopcroft, Department Chair

Department of Oceanography

Dr. S. Bradley Moran, Dean

College of Fisheries and Ocean Sciences

Dr. Michael Castellini

Dean of the Graduate School

Abstract

It has been hypothesized that climate change will reduce the strength and episodic nature of vernal phytoplankton blooms, increase heterotrophy of microbes and zooplankton, and weaken the tight coupling between pelagic and benthic production that is characteristic of Arctic continental shelves. As a part of the Arctic Shelf Growth, Advection, Respiration, and Deposition rates measurement (ASGARD) project, I quantified sinking particle fluxes and incubated sinking particles to measure the rate of microbial respiration associated with those particles. These measurements were used to characterize the strength of the pelagic-benthic connection. After a record-breaking year of warm temperatures and low-ice conditions in the northern Bering and southern Chukchi Seas, we observed massive vernal fluxes of sinking particulate organic carbon, ranking amongst the highest observed in the global oceans. Moreover, low rates of particle-associated microbial respiration indicate negligible recycling of sinking organic matter within the water column. These results suggest that the strength of the biological carbon pump may be maintained or enhanced in a warming Arctic, supporting strong benthic and upper trophic level productivity and carbon export.

Table of Contents

List of Figures

List of Supplementary Figures

List of Supplementary Tables

Acknowledgements

I would like to start by thanking the members of my graduate committee Sarah Hardy and Mark Johnson who have encouraged me, provided advice on data analysis, and help shape this thesis document. I am particularly grateful to my advisor, Andrew McDonnell, for accepting and funding me as his graduate student, for being available to me when I have questions, for offering great advice, and mostly for encouraging me to take ownership of this thesis project and working with me to figure out how to make my vision for this project come to reality, even though it was not part of his original proposal.

Financial support for this research was provided largely by the North Pacific Research Board, grant numbers G-11255 and G-12333. These grants comprise the ASGARD project and provided me with three semesters of research assistantships, summer funding, and paid for the field and lab work associated with this research. I was also supported by two semesters of teaching assistantships from the College of Fisheries and Ocean Sciences. Travel funding for conferences was provided by the Robert and Kathleen Byrd award and the North Pacific Research Board.

This research represents a collaborative effort. I would like to thank the Principal Investigators on the ASGARD project including Seth Danielson, Arny Blanchard, Sarah Hardy, Russ Hopcroft, Andrew McDonnell, and Dean Stockwell for conceiving of this larger ASGARD project. I am grateful for the flexibility of this group of people for allowing me to use ship time to deploy and recover drifting sediment traps even though it was not funded work. Of course this research would not have been possible without the competent, kind, and hard-working Captain, crew, and science technicians on the RV Sikuliaq. An additional thanks to all of the participants on the two ASGARD cruises. Many thanks to Dean Stockwell who conceived of and performed the field and lab work to collect the primary productivity rate measurements. Thanks also to Catherine Lalande and her lab who ran the samples from the moored sediment traps. In chapter 1 of this thesis, “we” refers to the intended coauthors of

this manuscript, Catherine Lalande, Dean Stockwell, Andrew McDonnell, and myself. Finally, thanks to the Alaska Stable Isotope Facility, especially Tim Howe, for training me on how to prepare samples and running many samples for particulate organic carbon and stable isotope analysis.

I would like to thank folks who provided materials and advice this thesis research. First, Russ Hopcroft for sharing his respiration measuring rig, including incubation chamber, oxygen reader, incubation vials, chiller, and software to read oxygen measurements. Russ also provided advice on how to analyzed respiration data used in this thesis. I would also like to thank Bradley Moran for donating all of the drifting sediment trap equipment used in this research. Thanks also to the whole McDonnell lab including Jess Pretty, Rachel Lekanoff, and Brita Irving for help preparing for talks at conferences and technical support on data analysis and making figures. This research would not have been possible without all of this assistance.

To all of my parents and grandparents and sister, thanks for the support from afar. To Tait, Kenya, and Meeko, thanks for moving to Fairbanks with me and providing emotional support and encouragement in our new home. Thanks to all of my kind, fun-loving, goofy friends in Fairbanks and all over the country. Lots of love to you all.

Chapter 1: General Introduction

The inventory of atmospheric carbon dioxide (CO_2) has increased on average 4 PgC yr^{-1}, constituting a 40% increase since the onset of the Industrial Revolution, largely due to burning of fossil fuel, cement production, and changing land use (France et al. 2013). Thus far, the ocean has acted as a net sink of CO_2, taking up 22% of total anthropogenic CO_2 emissions (Le Quéré et al. 2018). This carbon sequestration in the ocean is mostly due to the biological carbon pump (Sarmiento and Gruber 2006). If we are to understand global carbon cycling and the ramifications of climate change, the fate of carbon within the ocean must be better understood. It has been hypothesized that the ocean's ability to sequester additional CO_2 may decrease as atmospheric concentration of CO_2 continues to rise (France et al. 2013). Any changes in the strength of the biological carbon pump could have major implications for atmospheric concentration of CO_2.

1.1 The biological and physical carbon pumps

The biological carbon pump (BCP) is responsible for exporting particulate organic carbon (POC) out of surface waters, mainly through gravitational forces acting on sinking particles (Figure 1). In surface waters where sufficient light and nutrients are available, photoautotrophs (e.g., phytoplankton and cyanobacteria) convert dissolved inorganic carbon (DIC) into POC and dissolved organic carbon (DOC), and produce dissolved oxygen (DO) as a byproduct. Photosynthesis lowers partial pressure of CO_2 (pCO_2) at the air-sea interface, and allows for more diffusion of atmospheric CO_2 into the ocean. Photosynthetic organisms can then be consumed by zooplankton or killed by viral lysis where after their carbon is consumed by heterotrophic bacteria. Once consumed by heterotrophs, the organic carbon biomass is respired, consuming DO and producing DIC. Autotrophic respiration also produces DIC in surface waters. If these recycling mechanisms occur within the surface mixed layer of the ocean, surface DIC concentration increases. However, POC, unlike DIC, can sink through the water column. POC

that sinks to great depths in the ocean prior to being respired into DIC will remain sequestered from the atmosphere for a longer period of time, because upward diffusion of DIC occurs much more slowly than POC sinks through the water column via the gravitational carbon pump. Therefore, the depth at which POC is respired has implications for atmospheric CO_2 concentration (Kwon et al. 2009). The BCP operates over shorter timescales than thermohaline circulation, which also transports carbon to depth via the physical carbon pump. Without the BCP, atmospheric CO_2 would be 170 ppm higher than it is today (France et al. 2013). Therefore, it is critical to accurately quantify the BCP.

The BCP is measured as carbon flux, which is the rate at which carbon passes through the water column. Biogeochemists typically measure carbon flux in units of mg C m^{-2} d^{-1}. Flux is usually measured at the base of the euphotic zone, at various depths below that (e.g., every 100 – 1000 m below the euphotic zone), and ideally as a deposition rate on the seafloor. There are a variety of methods for estimating carbon flux, but the most common way to directly measure flux is to collect sinking particles in a sediment trap (McDonnell et al. 2015b). Sinking particles pass through an opening of known area, during a measured time period, and are funneled into a collection device containing preservative. One type of sediment trap is surface tethered, and drifts freely with the currents. These traps tend to be deployed for short durations (hours to days). The second type of sediment trap is moored, or bottom tethered. These traps are stationary, and typically deployed for longer timescales (months to years). They usually have multiple collection containers, which rotate on a preprogrammed time frame, allowing flux to be measured during discrete time intervals. The third most common type of sediment traps are neutrally buoyant traps, which are deployed at a certain pressure corresponding with a certain depth and maintain that pressure, eliminating surface wave action. They also drift with a water mass and are often deployed for days. Neutrally buoyant traps are considered best-practice for calculating flux (Buesseler et al. 2007), because they eliminate some of the hydrodynamic biases associated with the other two designs. However, neutrally buoyant traps cannot be deployed in shallow coastal water.

At current speeds over 12 cm s^{-1}, moored traps under-collect sinking particles by over 75% in comparison with freely drifting cylindrical traps (Baker et al. 1988). Regardless of which platform is used, cylindrical or conical cylindrical collection tubes with high aspect ratios (height:diameter) reduce the likelihood of flushing associated with funnel-shaped collection devices (Buesseler et al. 2007). Baffles on conical funnels also help mitigate flushing.

Determining the rate of respiration associated with sinking particles allows for better predictions of how deep POC can sink before it is respired into DIC below the depths at which sediment traps can be easily deployed. There are various approaches for measuring these rates. One approach is using in situ RESPIRE traps, which collect sinking particles and incubate them at depth in the ocean, measuring bulk change in oxygen over time (Boyd et al. 2015; McDonnell et al. 2015a). These traps measure rates with the least amount of disruption to particles, which are delicate. Some disruption does still occur due to arresting sinking, which can change the exchange of oxygen between particle and surrounding water. Particles also can aggregate with each other at the bottom of the trap changing oxygen exchange dynamics. Additionally, there is relatively little labor involved and good reproducibility of measurements. However, it is hard to correct for respiration of swimmers, which could also consume particles during the incubation. Additionally, these instruments are expensive and challenging to deploy and recover. Another method is measuring oxygen gradients of individual sinking particles (Belcher et al. 2016b). This method allows for per particle respiration rate measurement, by measuring the strength of the gradient of oxygen concentration from the inside to the outside of the particle to calculate the particle remineralization rate. Removing zooplankton swimmers is easy with this method. Unfortunately, this is the most labor intensive method and requires the most disruption of particles, possibly altering true respiration rates. Additionally, these measurements are often only done on large aggregates, and therefore require additional assumptions to convert to bulk sinking particle remineralization. A third method of measuring respiration rates of sinking particles is bulk incubation of

sinking particles collected using short-term sediment traps (Collins et al. 2015). This method represents a compromise between particle disruption, reproducibility, and labor intensity. Unfortunately, respiration rate measurements of sinking particles are rare because they are labor intensive and/or expensive.

There are some general spatial trends in respiration rates of sinking particles. Respiration rates tend to be higher in tropical regions. As a part of the Bermuda Atlantic Time-series Study (BATS), particle-associated microbial (PAM) respiration rates were measured at 0.4 +/- 0.1 day^{-1}, meaning that 40 +/- 10% of POC was respired per day (McDonnell et al. 2015a). A few studies in the North Atlantic found PAM rates around 0.007 +/- 0.003 to 0.173+/- 0.105 day^{-1} and 0.002 – 0.030 day^{-1}, substantially lower than rates at BATS (Collins et al. 2015; Belcher et al. 2016a). Respiration rates in Antarctic Scotia Sea were also much lower than the rates at BATS, ranging from 0.010 – 0.065 day^{-1} and averaging 0.028 day^{-1} (Belcher et al. 2016b). Finally, at the west Antarctic Peninsula (WAP), no significant PAM could be detected (McDonnell et al. 2015a). This decrease in PAM rate at higher latitudes is likely influenced by temperature effects on respiration as well as the nature of the organic matter and its protection by biogenic minerals or peritrophic membranes (Sarmiento and Gruber 2006). This pattern of decreasing PAM at higher latitudes helps support efficient high-latitude food webs, with minimal organic matter recycling in the euphotic zone and tighter pelagic-benthic coupling at high latitudes.

The efficiency of the BCP can be estimated by calculating an export ratio (e-ratio) using direct measurements of POC flux at the base of the euphotic zone and primary productivity integrated through the euphotic zone (Equation 1).

$$e-ratio = \frac{Flux}{PP} * 100\% \qquad \textit{Equation 1}$$

A typical e-ratio in the open ocean is about 10%, compared to 25% in coastal waters (Dunne et al. 2005, 2007). Lower e-ratios characterize ecosystems with more organic matter recycling in the euphotic zone, whereas higher e-ratios occur in regions where freshly produced POC is efficiently exported out of the euphotic zone. Some coastal systems have highly efficient export, with e-ratios reaching 100% (Le Moigne et al. 2013). It should be noted that some amount of spatial and/or temporal decoupling of PP and flux always exists, which is demonstrated in e-ratios that exceed 100% (Moran et al. 2012; Baumann et al. 2013; Le Moigne et al. 2015), for example due to horizontal displacement of particles by currents which can be orders of magnitude faster than particle sinking speeds in coastal areas (Gustafsson et al. 1998). In addition, a temporal offset can occur between peak primary production and peak flux due to slow particle sinking rates. If sampling occurs after peak primary production has occurred, and remineralization rates within the euphotic zone are low, e-ratios can exceed 100%. The magnitude of spatial and temporal decoupling should be considered with all e-ratio measurements.

1.2 Continental shelves and carbon cycling

Although the largest reservoirs of carbon are found in the deep ocean due to the long time scales at which carbon is sequestered in deep water, 86% of all carbon deposition and 91% of all carbon burial in ocean sediments occurs on continental shelves, making them critical regions for parameterizing carbon cycling in the ocean (Sarmiento and Gruber 2006). In addition, large quantities of carbon are laterally exported from shelves into the deep ocean (O'Brien et al. 2006; Buesseler et al. 2010). Thus, shelves are disproportionately responsible for POC export away from surface waters. High productivity that occurs on continental shelves (due to high nutrient availability and coastal upwelling in some regions) and faster transport to the seafloor through the shallow water column, coupled with less microbial degradation are responsible for POC high sedimentation rates on continental shelves. Higher deposition to the sediments also enhances carbon burial because the large supply of labile carbon is

rapidly remineralized and relatively quickly buried as recalcitrant material, leading to a shallow layer of anoxic sediments where further microbial degradation is relatively slow (Sarmiento and Gruber 2006). However, currents can be very fast in these shallow waters, causing horizontal advection of sinking particles as well as resuspension of particles that have already settled to the seafloor (Gustafsson et al. 1998; Abe et al. 2019). All of these factors present challenges for measuring flux on shallow shelves. Despite these challenges, these regions must be studied because of their disproportionate responsibility for sequestering atmospheric CO_2.

1.3 The Bering and Chukchi shelves

The northern Bering and southern Chukchi seas overlie a large, seasonally ice-covered shallow shelf (Grebmeier 2012) (Figure 2). After ice retreat during the late spring, nutrient rich Anadyr waters fuel some of the highest rates of primary production on earth (Walsh et al. 1989; Springer and McRoy 1993). In fact, the highest rate of PP that has been measured globally, 16 g C m^{-2} d^{-1}, occurred on the Chukchi Sea shelf (Walsh et al. 1989; Springer and McRoy 1993). Phytoplankton blooms are mostly characterized by the diatoms *Thalassiosira* spp. and *Chaetocerus* spp. (Springer and McRoy 1993). Large calanoid copepods are advected onto the shelf from the North Pacific, and smaller-bodied shelf-dwelling copepods are typical zooplankton grazers in this system; however, zooplankton are not thought to play a major role in carbon cycling in this region (Walsh et al. 1989; Campbell et al. 2009; Hopcroft et al. 2010). The Bering and Chukchi Sea shelves have the highest benthic biomass in the Arctic (Grebmeier and McRoy 1988), mostly consisting of ampeliscid amphipods, bivalves and other invertebrates (Grebmeier and McRoy 1988, 1989). This direct connection between pelagic primary production and benthic productivity is referred to as tight pelagic-benthic coupling, which supports rich benthic secondary productivity (Grebmeier and Barry 1991; Grebmeier 2012). High benthic biomass is transferred to upper trophic levels through consumption by grey whales and walrus as well as diving ducks and other seabirds

(Lowry and Frost 1981; Grebmeier et al. 2006). These predators support subsistence hunting on the West coast of Alaska, St. Lawrence Island, the Diomede Islands, as well as on the East coast of Siberia.

Tight pelagic-benthic coupling provides the framework for the ecology and carbon cycling of this region, indicating a strong and efficient BCP (i.e., large amounts of carbon sink through the water column and reach the seafloor relatively undegraded). Sediment chlorophyll-a concentration, total organic carbon (TOC), and sediment community oxygen consumption have been compared with overlying primary production to infer spatial and temporal patterns in particulate carbon flux (Grebmeier and McRoy 1989; Grebmeier et al. 2006; Cooper et al. 2012; Grebmeier 2012). These water column/sediment comparisons suggest this region has the second highest carbon deposition rate globally (Pipko et al. 2002; Chen et al. 2014). High quality food that settles on the seafloor during the spring and summer fuels benthic productivity all year (Pirtle-Levy et al. 2009).

Despite the tight pelagic-benthic coupling described in this region, few studies have directly measured carbon flux or deposition rates on the Bering and Chukchi shelves. One moored sediment trap study conducted in summer 1988 collected 8-day averaged flux measurements on the Bering Sea shelf about 500 miles south of the Bering Strait (Fukuchi et al. 1993), and estimated flux at about 501 mg C m^{-2} d^{-1}. This rate roughly matched estimates derived from comparing primary production with sediment oxygen uptake converted to carbon demand: about 464 mg C m^{-2} d^{-1} (Grebmeier and McRoy 1989). One additional flux calculation from the Chukchi Sea shelf in August 1994 using the Thorium-234/Uranium-238 disequilibrium method was very similar in magnitude: 456 mg C m^{-2} d^{-1} (Moran et al. 1997). Several additional measurements of flux have been reported for the shelf breaks and slope areas in the Bering and Chukchi seas (Moran et al. 2005, 2012; Lalande et al. 2007; Lepore et al. 2007; Baumann et al. 2013), however, no other measurements have been reported on the shallow shelf where PP is highest and flux is likely highest as well (Grebmeier et al. 2006).

It is important to consider carbon cycling within the context of strong lateral advection when determining timescales of carbon sequestration in this region. The Bering Strait is a constriction for northward flowing currents. This region can experience bottom current speeds over 1 m s^{-1}, especially in the fall (Roach et al. 1995). For example, in a 50-m water column with currents of 1 m s^{-1}, a particle sinking 50 m d^{-1} will travel 86.4 kilometers horizontally before reaching the seafloor. Fast bottom currents also cause resuspension of particles from the seafloor. Abe et al. (2019) hypothesized that resuspension events in the Bering Sea and subsequent resettling of POC are responsible for benthic hotspots found north of the Bering Strait (Grebmeier et al. 2015). POC and DIC can also be advected off the shelf into the deep Arctic Basin, where it can be considered "sequestered" (Dunton et al. 2005; Bates 2006). In fact, Moran et al. (2005) found that up to 20% of net primary production (NPP) on the Chukchi Sea shelf is advected off shelf in the summer. However, fall storms can disrupt sequestration to the deep Arctic by mixing the water column and allowing for outgassing of DIC to the atmosphere (Hauri et al. 2013).

1.4 Climate Change and the Arctic

There are many physical parameters substantiating the claims that the Arctic is changing rapidly due to global climate change. Arctic surface air temperature has warmed twice as quickly as subpolar regions, much more quickly than expected (Osborne et al. 2018). Each of the twelve years from 2006 to 2018 ranks in the top twelve lowest summer sea ice extents on record. Additionally, ice thinning, reduced winter ice extents, longer ice-free period, and decreased multiyear ice have been observed (Johnson and Eicken 2016).

A major debate within the scientific community is revolving around how physical changes in the Arctic due to global climate change will affect the chemistry and biology of this region and what the potential global ramifications are for those physical changes. One hypothesis that emerged from the

well-studied European Arctic Shelf near Svalbard is that an Arctic with a longer open water season will have elongated pelagic phytoplankton blooms, potentially limited by nutrients and therefore reaching a lower peak magnitude (Wassmann and Reigstad 2011). So far Arctic pelagic primary productivity in general has increased with climate change, some say by up to 30% from 1998 to 2012 (Arrigo et al. 2008; Arrigo and van Dijken 2015), due to a longer ice-free season. However, it's possible that in the future temperature may warm to a point that increased stratification causes nutrient limitation to the point of decreased PP (Fu et al. 2016). Future changes in dominant phytoplankton species in the Arctic could also have major implications for Arctic primary production (Comeau et al. 2011; Riebesell et al. 2013; Fujiwara et al. 2014; Paulsen et al. 2016). Scientists still cannot accurately predict how primary production in the Arctic will be affected by climate change.

In addition to effects on primary production, climate change may affect water-column cycling of organic carbon, potentially altering the tight pelagic-benthic coupling characteristic of certain Arctic shelves, such as the Bering, Chukchi, and Barents seas (Piepenburg 2005; Wassmann and Reigstad 2011). Increased heterotrophy in the water column due to warmer temperatures, better matched timing of zooplankton and phytoplankton productivity, and a potential shift to sub-arctic grazers with higher metabolic demand are all predicted to weaken pelagic-benthic coupling by decreasing flux to the benthos (Coyle et al. 2007; Wassmann and Reigstad 2011). Moore and Stabeno (2015) predict a shift from a benthic dominated past to a pelagic dominated future as a result of these changes in the Bering and Chukchi seas (Figure 3). A weakening of the pelagic-benthic coupling would have major implications for the ecology of the Bering and Chukchi shelves. Grebmeier et al. (2006) concludes that short food chains characteristic of the Bering and Chukchi shelves are particularly vulnerable to changes, as changes to fitness of ice-dependent apex predators opens a large niche to an ecosystem-wide trophic reorganization. Therefore, it is critical to determine what changes are occurring to pelagic-benthic coupling in the Bering and Chukchi seas.

1.5 The ASGARD Study

The Arctic Shelf Growth, Advection, Respiration and Deposition Rates measurement project (ASGARD) consisted of cruises during June of 2017 and 2018 aboard the R/V Sikuliaq. These two cruises were the basis for my field measurements. The major objectives of this thesis research are to determine 1) carbon flux, primary production, and export efficiency on the Pacific-Arctic shelf and how they compare to previous measurements from this region and globally; and 2) the role of PAM in recycling POC within the water column.

The largest blooms in the Bering and Chukchi shelves occur immediately after ice retreat in the late spring (Grebmeier and McRoy 1988; Cooper et al. 2012), however most sampling in this region occurs in the late summer or early fall. Additionally, the strength of the BCP is often inferred by coupling sediment processes with water column nutrient and/or productivity rates (Grebmeier and McRoy 1989) without directly measuring export flux or water-column PAM respiration rates. Finally, rapid changes occurring in this region, and the Arctic as a whole, signal that this is a critical time to fill in these data gaps and more accurately quantify carbon cycling on the Bering and Chukchi shelves (Figure 4). These are all motivations driving this thesis research to determine the strength and efficiency of the biological carbon pump on the Pacific-Arctic shelf. The following chapter and appendix are drafted for submission to Science Research Articles.

1.6 References

Abe H, Sampei M, Hirawake T, et al. (2019) Sediment-associated phytoplankton release from the seafloor in response to wind-induced barotropic currents in the Bering Strait. Front Mar Sci 6:1–9. https://doi.org/10.3389/fmars.2019.00097

Arrigo KR, van Dijken G, Pabi S (2008) Impact of a shrinking Arctic ice cover on marine primary production. Geophys Res Lett 35:1–6. https://doi.org/10.1029/2008GL035028

Arrigo KR, van Dijken GL (2015) Continued increases in Arctic Ocean primary production. Prog Oceanogr 136:60–70. https://doi.org/10.1016/j.pocean.2015.05.002

Baker ET, Milburn HB, Tennant DA (1988) Field assessment of sediment trap efficiency under varying flow conditions. J Mar Res 46:573–592. https://doi.org/10.1357/002224088785113522

Bates NR (2006) Air-sea CO_2 fluxes and the continental shelf pump of carbon in the Chukchi Sea adjacent to the Arctic Ocean. J Geophys Res Ocean 111:1–21. https://doi.org/10.1029/2005JC003083

Baumann MS, Moran SB, Lomas MW, et al. (2013) Seasonal decoupling of particulate organic carbon export and net primary production in relation to sea-ice at the shelf break of the eastern Bering Sea: Implications for off-shelf carbon export. J Geophys Res Ocean 118:5504–5522. https://doi.org/10.1002/jgrc.20366

Belcher A, Iversen M, Giering S, et al. (2016a) Depth-resolved particle-associated microbial respiration in the northeast Atlantic. Biogeosciences 13:4927–4943. https://doi.org/10.5194/bg-13-4927-2016

Belcher A, Iversen M, Manno C, et al. (2016b) The role of particle associated microbes in remineralization of fecal pellets in the upper mesopelagic of the Scotia Sea, Antarctica. Limnol Oceanogr 61:1049–1064. https://doi.org/10.1002/lno.10269

Boyd PW, McDonnell A, Valdez J, et al. (2015) RESPIRE: An in situ particle interceptor to conduct particle remineralization and microbial dynamics studies in the oceans' Twilight Zone. Limnol Oceanogr Methods 13:494–508. https://doi.org/10.1002/lom3.10043

Buesseler KO, Chen M, Harada K, et al. (2007) An assessment of the use of sediment traps for estimating upper ocean particle fluxes. J Mar Res 65:345–416. https://doi.org/10.1357/002224007781567621

Buesseler KO, McDonnell AMP, Schofield OME, et al. (2010) High particle export over the continental shelf of the west Antarctic Peninsula. Geophys Res Lett 37:1–5. https://doi.org/10.1029/2010GL045448

Campbell RG, Sherr EB, Ashjian CJ, et al. (2009) Mesozooplankton prey preference and grazing impact in the western Arctic Ocean. Deep-Sea Res II. https://doi.org/10.1016/j.dsr2.2008.10.027

Chen L, Gao Z, Sun H, et al. (2014) Distributions and air-sea fluxes of CO_2 in the summer Bering Sea. Acta Oceanol Sin 33:1–8. https://doi.org/10.1007/s13131-014-0483-9

Collins JR, Edwards BR, Thamatrakoln K, et al. (2015) The multiple fates of sinking particles in the North Atlantic Ocean. Global Biogeochem Cycles 29:1471–1494. https://doi.org/10.1002/2014GB005037.Received

Comeau AM, Li WKW, Tremblay JÉ, et al. (2011) Arctic ocean microbial community structure before and after the 2007 record sea ice minimum. PLoS One 6:e27492. https://doi.org/10.1371/journal.pone.0027492

Cooper LW, Janout MA, Frey KE, et al. (2012) The relationship between sea ice break-up, water mass variation, chlorophyll biomass, and sedimentation in the northern Bering Sea. Deep Res II 65–70:141–162. https://doi.org/10.1016/j.dsr2.2012.02.002

Coyle KO, Bluhm B, Konar B, et al. (2007) Amphipod prey of gray whales in the northern Bering Sea: Comparison of biomass and distribution between the 1980s and 2002-2003. Deep-Sea Res II 54:2906–2918. https://doi.org/10.1016/j.dsr2.2007.08.026

Dunne JP, Armstrong RA, Gnnadesikan A, Sarmiento JL (2005) Empirical and mechanistic models for the particle export ratio. Global Biogeochem Cycles 19:1–16. https://doi.org/10.1029/2004GB002390

Dunne JP, Sarmiento JL, Gnanadesikan A (2007) A synthesis of global particle export from the surface ocean and cycling through the ocean interior and on the seafloor. Global Biogeochem Cycles 21:1–16. https://doi.org/10.1029/2006GB002907

Dunton KH, Goodall JL, Schonberg S V., et al. (2005) Multi-decadal synthesis of benthic-pelagic coupling in the western arctic: Role of cross-shelf advective processes. Deep-Sea Res II 52:3462–3477. https://doi.org/10.1016/j.dsr2.2005.09.007

France PC, Willem J, Friedlingstein P, Munhoven G (2013) Intergovernmental Panel on Climate Change. Climate change 2013: Carbon and other biogeochemical cycles. Working Group I Contribution to IPCC fifth Assessment Report. https://doi.org/10.1017/CBO9781107415324.015

Fu W, Randerson JT, Keith Moore J (2016) Climate change impacts on net primary production (NPP) and export production (EP) regulated by increasing stratification and phytoplankton community structure in the CMIP5 models. Biogeosciences. https://doi.org/10.5194/bg-13-5151-2016

Fujiwara A, Hirawake T, Suzuki K, et al. (2014) Timing of sea ice retreat can alter phytoplankton community structure in the western Arctic Ocean. Biogeosciences. https://doi.org/10.5194/bg-11-1705-2014

Fukuchi M, Sasaki H, Hattori H, et al. (1993) Temporal variability of particulate flux in the northern Bering Sea. Cont Shelf Res 13:693–704. https://doi.org/10.1016/0278-4343(93)90100-C

Grebmeier JM (2012) Shifting patterns of life in the Pacific Arctic and Sub-Arctic Seas. Ann Rev Mar Sci 4:63–78. https://doi.org/10.1146/annurev-marine-120710-100926

Grebmeier JM, Barry JP (1991) The influence of oceanographic processes on pelagic-benthic coupling in polar regions : A benthic perspective. J Mar Syst 2:495–518

Grebmeier JM, Bluhm BA, Cooper LW, et al. (2015) Ecosystem characteristics and processes facilitating persistent macrobenthic biomass hotspots and associated benthivory in the Pacific Arctic. Prog Oceanogr 136:92–114. https://doi.org/10.1016/j.pocean.2015.05.006

Grebmeier JM, Cooper LW, Feder HM, Sirenko BI (2006) Ecosystem dynamics of the Pacific-influenced Northern Bering and Chukchi Seas in the Amerasian Arctic. Prog Oceanogr 71:331–361. https://doi.org/10.1016/j.pocean.2006.10.001

Grebmeier JM, McRoy CP (1988) Pelagic-benthic coupling on the shelf of the northern Bering and Chukchi Seas. I. Food supply and source and benthic biomass. Mar Ecol Prog Ser 48:57–67. https://doi.org/10.3354/meps053079

Grebmeier JM, McRoy CP (1989) Pelagic-benthic coupling on the shelf of the northern Bering and Chukchi Seas. III. Benthic food supply and carbon cycling. Mar Ecol Prog Ser 53:93–100. https://doi.org/0171-8630/89/0053/0079/$ 03.00

Gustafsson Ö, Buesseler KO, Geyer WR, et al. (1998) An assessment of the relative importance of horizontal and vertical transport of particle-reactive chemicals in the coastal ocean. Cont Shelf Res. https://doi.org/10.1016/S0278-4343(98)00015-6

Hauri C, Winsor P, Juranek LW, et al. (2013) Wind-driven mixing causes a reduction in the strength of the continental shelf carbon pump in the Chukchi Sea. Geophys Res Lett 40:5932–5936. https://doi.org/10.1002/2013GL058267

Hopcroft RR, Kosobokova KN, Pinchuk AI. (2010) Zooplankton community patterns in the Chukchi Sea during summer 2004. Deep-Sea Res II 57:27-39. https://doi.org/10.1016/j.dsr2.2009.08.003

Johnson M, Eicken H (2016) Estimating Arctic sea-ice freeze-up and break-up from the satellite record: A comparison of different approaches in the Chukchi and Beaufort Seas. Elementa. https://doi.org/10.12952/journal.elementa.000124

Kwon EY, Primeau F, Sarmiento JL (2009) The impact of remineralization depth on the air–sea carbon balance. Nat Geosci 2:630–635. https://doi.org/10.1038/ngeo612

Le Quéré C, Andrew R, Friedlingstein P, et al. (2018) Global Carbon Budget 2018. Earth Syst Sci Data 10:2141–2194. https://doi.org/10.5194/essd-10-2141-2018

Lalande C, Lepore K, Cooper LW, et al. (2007) Export fluxes of particulate organic carbon in the Chukchi Sea: A comparative study using $^{234}Th/^{238}U$ disequilibria and drifting sediment traps. Mar Chem 103:185–196. https://doi.org/10.1016/j.marchem.2006.07.004

Le Moigne FAC, Henson SA, Sanders RJ, Madsen E (2013) Global database of surface ocean particulate organic carbon export fluxes diagnosed from the ^{234}Th technique. Earth Syst Sci Data 5:295–304. https://doi.org/10.5194/essd-5-295-2013

Le Moigne FAC, Poulton AJ, Henson SA, et al. (2015) Carbon export efficiency and phytoplankton community composition in the Atlantic sector of the Arctic Ocean. AGU Publ 120:3896–3912. https://doi.org/10.1002/2015JC010700

Lepore K, Moran SB, Grebmeier JM, et al. (2007) Seasonal and interannual changes in particulate organic carbon export and deposition in the Chukchi Sea. J Geophys Res Ocean 112:1–14. https://doi.org/10.1029/2006JC003555

Lowry LF, Frost KJ (1981) Distribution, growth, and foods of Arctic cod (*Boreogadus saida*) in the Bering, Chukchi and Beaufort Seas. Can Field-Naturalist 95(2):186-191.

McDonnell AMP, Boyd PW, Buesseler KO (2015a) Effects of sinking velocities and microbial respiration rates on the attenuation of particulate carbon fluxes through the mesopelagic zone. Global Biogeochem Cycles 29:175–193. https://doi.org/10.1002/2014GB004935.Received

McDonnell AMP, Lam PJ, Lamborg CH, et al. (2015b) The oceanographic toolbox for the collection of sinking and suspended marine particles. Prog Oceanogr 133:17–31. https://doi.org/10.1016/j.pocean.2015.01.007

Moore SE, Stabeno PJ (2015) Synthesis of Arctic Research (SOAR) in marine ecosystems of the Pacific Arctic. Prog Oceanogr 136:1–11. https://doi.org/10.1016/j.pocean.2015.05.017

Moran SB, Ellis KM, Smith JN (1997) $^{234}Th/^{238}U$ disequilibrium in the central Arctic Ocean: Implications for particulate organic carbon export. Deep-Sea Res II 44:1593–1606. https://doi.org/10.1016/S0967-0645(97)00049-0

Moran SB, Kelly RP, Hagstrom K, et al. (2005) Seasonal changes in POC export flux in the Chukchi Sea and implications for water column-benthic coupling in Arctic shelves. Deep-Sea Res II 52:3427–3451. https://doi.org/10.1016/j.dsr2.2005.09.011

Moran SB, Kelly RP, Iken K, et al. (2012) Seasonal succession of net primary productivity, particulate organic carbon export, and autotrophic community composition in the eastern Bering Sea. Deep-Sea Res II 65–70:84–97. https://doi.org/10.1016/j.dsr2.2012.02.011

O'Brien MC, Macdonald RW, Melling H, Iseki K (2006) Particle fluxes and geochemistry on the Canadian Beaufort Shelf: Implications for sediment transport and deposition. Cont Shelf Res 26:41–81. https://doi.org/10.1016/j.csr.2005.09.007

Osborne E, Richter-Menge J, Jeffries M (2018) Arctic Report Card 2018, https://www.arctic.noaa.gov/Report-Card

Paulsen ML, Doré H, Garczarek L, et al. (2016) *Synechococcus* in the Atlantic Gateway to the Arctic Ocean. Front Mar Sci. https://doi.org/10.3389/fmars.2016.00191

Piepenburg D (2005) Recent research on Arctic benthos: Common notions need to be revised. Polar Biol 28:733–755. https://doi.org/10.1007/s00300-005-0013-5

Pipko II, Semiletov IP, Tishchenko PY, et al. (2002) Carbonate chemistry dynamics in Bering Strait and the Chukchi Sea. Prog Oceanogr 55:77–94. https://doi.org/10.1016/S0079-6611(02)00071-X

Pirtle-Levy R, Grebmeier JM, Cooper LW, Larsen IL (2009) Chlorophyll a in Arctic sediments implies long persistence of algal pigments. Deep-Sea Res II 56:1326–1338. https://doi.org/10.1016/j.dsr2.2008.10.022

Riebesell U, Gattuso JP, Thingstad TF, Middelburg JJ (2013) Preface arctic ocean acidification: Pelagic ecosystem and biogeochemical responses during a mesocosm study. Biogeosciences 10:5619–5626. https://doi.org/10.5194/bg-10-5619-2013

Roach AT, Aagaard K, Pease CH, et al. (1995) Direct measurements of transport and water properties through the Bering Strait. J Geophys Res 100:1844–18457. https://doi.org/10.1029/95JC01673

Sarmiento JL, Gruber N (2006) Ocean Biogeochemical Dynamics. Princeton University Press, Princeton, NJ

Springer AM, McRoy CP (1993) The paradox of pelagic food webs in the northern Bering Sea-III. Patterns of primary production. Cont Shelf Res 13:575–599. https://doi.org/10.1016/0278-4343(93)90095-F

Walsh JJ, McRoy CP, Coachman LK, et al. (1989) Carbon and nitrogen cycling within the Bering/Chukchi Seas: Source regions for organic matter effecting AOU demands of the Arctic Ocean. Prog Oceanogr 22:277–359. https://doi.org/10.1016/0079-6611(89)90006-2

Wassmann P, Reigstad M (2011) Future Arctic Ocean seasonal ice zones and implications for pelagic-benthic coupling. Oceanography 24:220–231

1.7 Figures

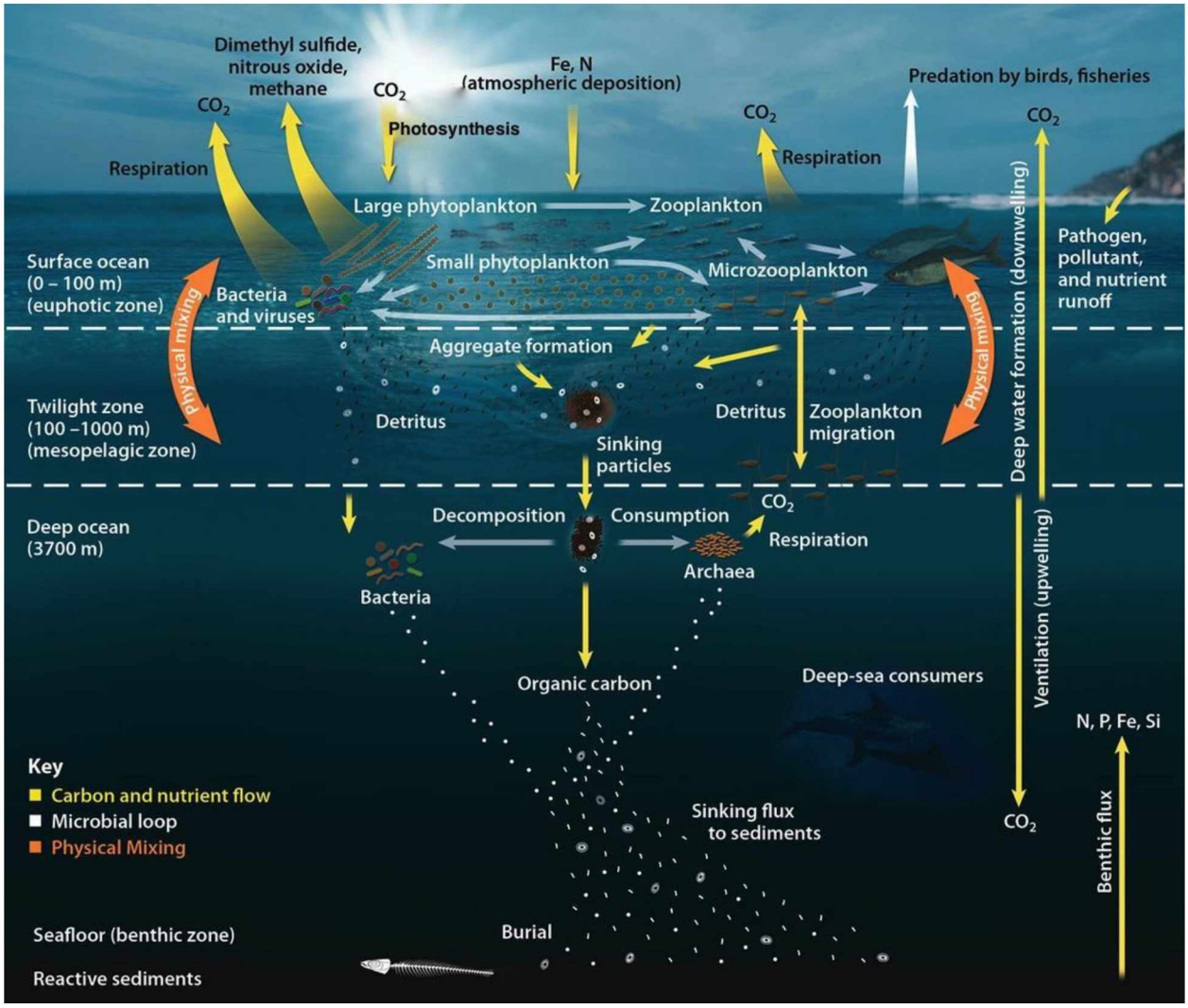

Figure 1.1. The Biological Carbon Pump. Image credit: Oak Ridge National Laboratory

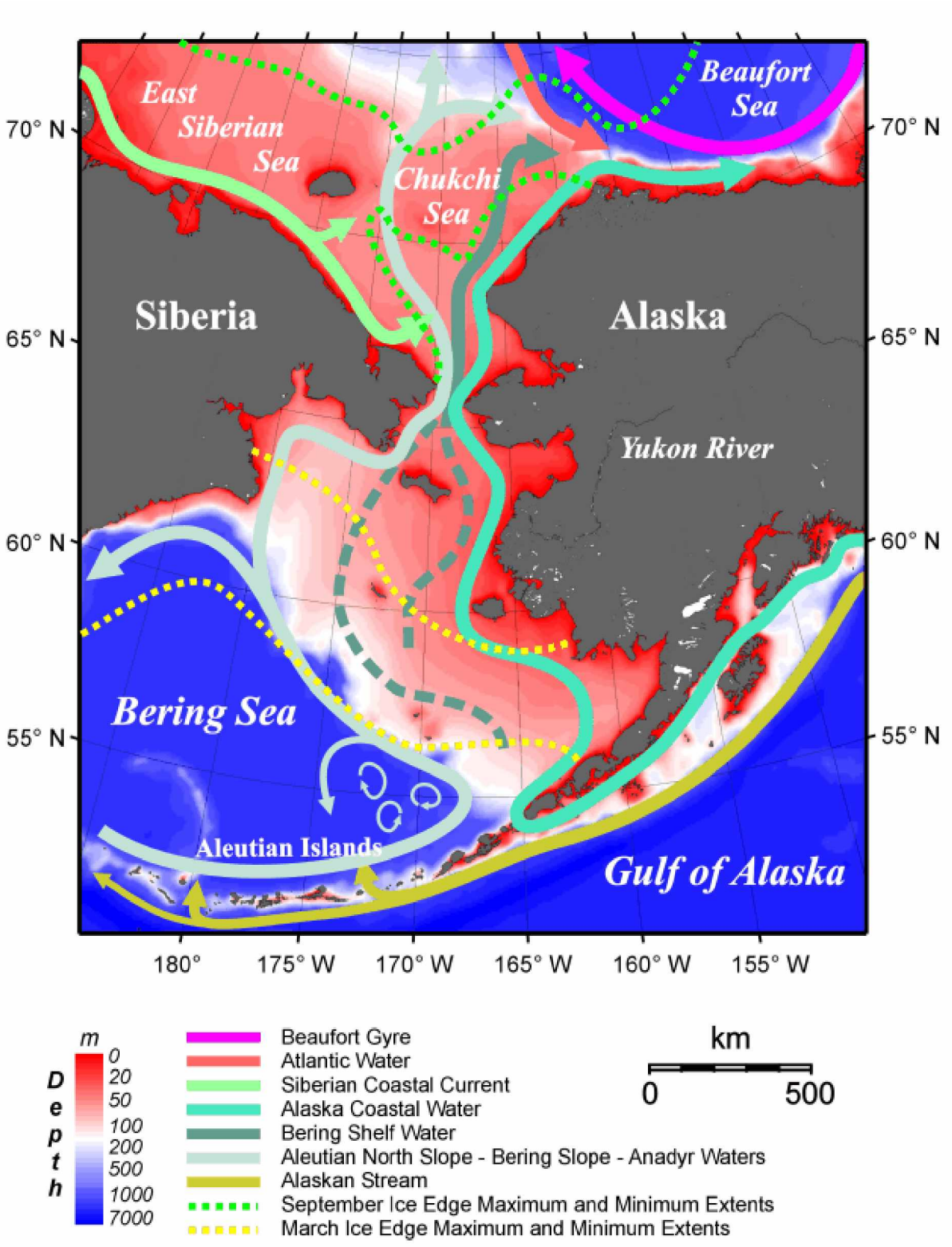

Figure 1.2. Major currents and water masses in the Bering and Chukchi seas (Weingartner and Danielson, UAF).

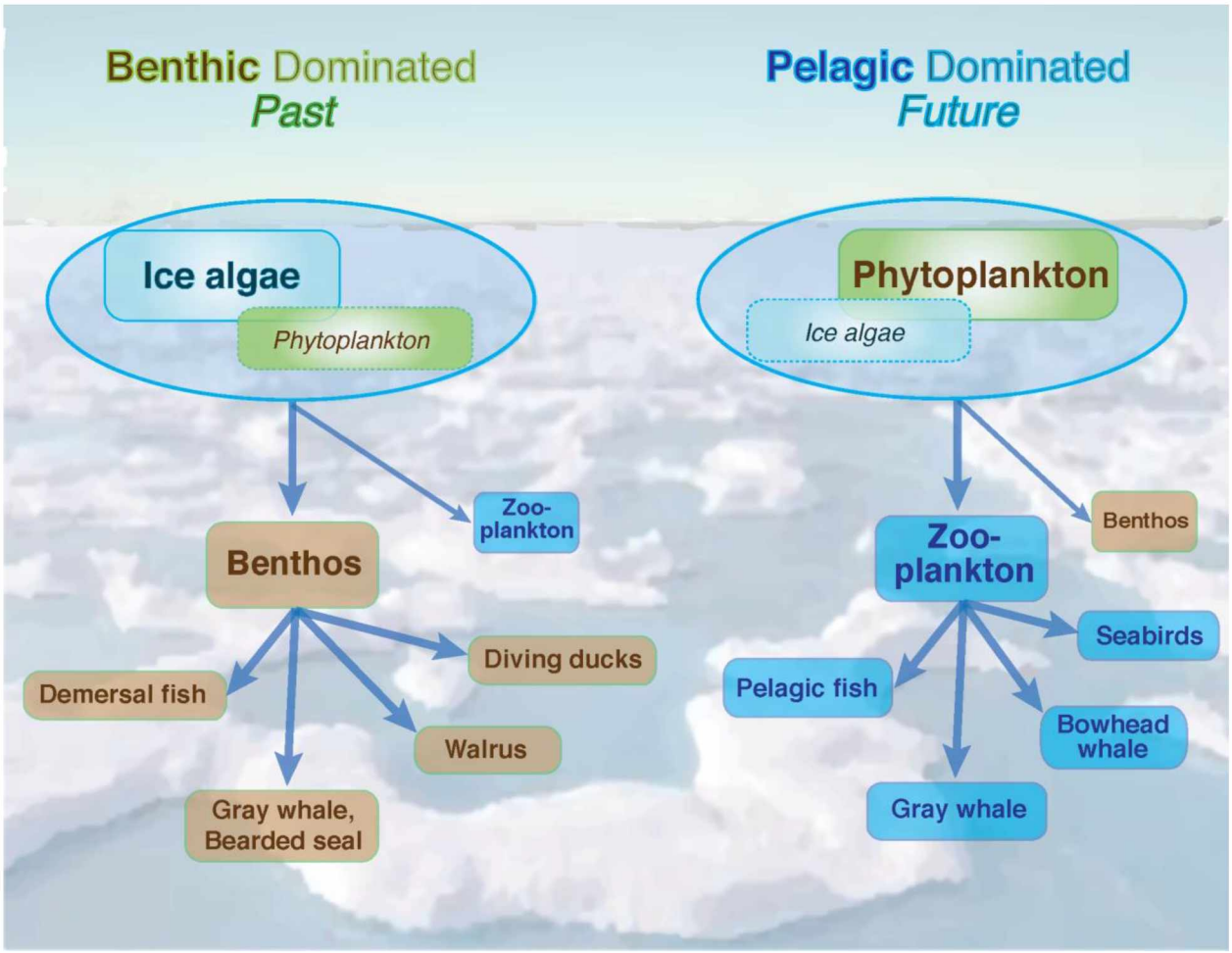

Figure 1.3. Pelagic-benthic coupling in the new Arctic. Hypothesis from Moore and Stabeno (2015) about how trophic transfer will change on the Bering and Chukchi shelves with climate change

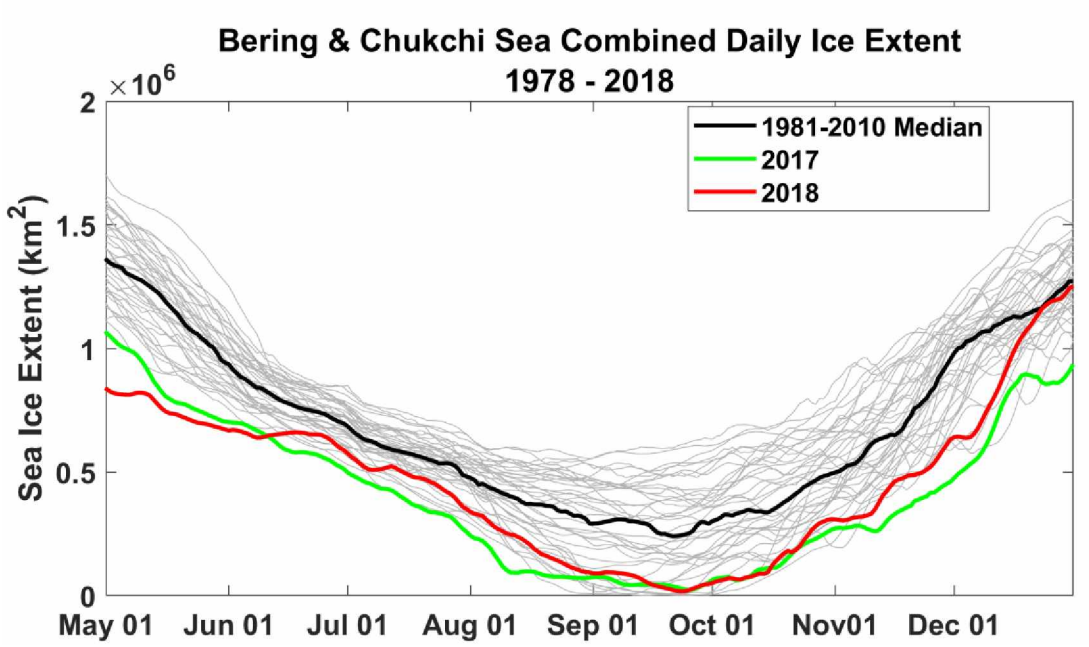

Figure 1.4. Bering and Chukchi Sea combined daily ice extent from 1978 to 2018 (data from NSDIC Ice Index). 2017 and 2018 had the two lowest sea ice extents on record, especially prominent in May of these years.

Chapter 2 -- Extraordinary carbon fluxes associated with warming and sea ice loss on the Pacific Arctic shelf[1]

[1] O'Daly, S.H., Lalande, C., Stockwell, D., & McDonnell, A.M.P. In preparation for Science Research Articles.

2.1 Abstract

Climate change may reduce the strength and episodic nature of vernal phytoplankton blooms, increase heterotrophy, and weaken the tight coupling between pelagic and benthic production that is characteristic of Arctic continental shelves. However, in the midst of two record-breaking years of warm temperatures and low-ice conditions during 2017 and 2018 within the northern Bering and southern Chukchi Seas, we observed massive vernal fluxes of sinking particulate organic carbon, ranking amongst the highest ever observed in the global oceans. Moreover, low rates of particle-associated microbial respiration indicate negligible recycling of sinking particulate organic carbon within the water column. These results suggest that the strength of the biological carbon pump may be maintained or enhanced in a warming Arctic, supporting strong benthic and upper trophic-level productivity and carbon export.

2.2 Introduction, Results, Discussion, and Conclusion

Arctic marine systems are currently undergoing rapid and profound changes due to the effects of climate change, including reduced sea ice extent, earlier sea ice retreat, protracted ice-free seasons, warming air and ocean temperatures, and shifts in currents and water column stratification (Vaughan et al. 2013; Osborne et al. 2018). These environmental changes have recently accelerated on the Pacific Arctic shelf that includes the Bering and Chukchi Seas, with several consecutive years of record-breaking ocean and air temperatures, and an unprecedented dearth of sea ice (Stabeno and Bell 2019). Cascading impacts on regional ecosystems, biogeochemical cycles, climate, and human communities are expected, although, at present, the nature and magnitude of these impacts remain largely speculative.

The continental shelves of the Arctic, and particularly the shallow Pacific Arctic shelf, are among the marine ecosystems with the highest pelagic primary productivity and carbon sedimentation rates anywhere on Earth (Walsh et al. 1989; Springer and McRoy 1993; Pipko et al. 2002; Chen et al. 2014). Productivity in the Pacific Arctic is fueled by abundant light and the northward advection of nutrient-rich water masses of Pacific origins (Danielson et al. 2017). The spring phytoplankton bloom is typically

dominated by large, quickly-sinking ice-associated or pelagic diatoms (Springer and McRoy 1993; Gradinger 1999, 2009). Much of this production is deposited on the underlying sediments in large quantities (Pipko et al. 2002; Chen et al. 2014), supporting one of the most productive benthic ecosystems on Earth (Grebmeier and McRoy 1988, 1989). This rich benthic biomass, in turn, feeds large populations of benthic-feeding pelagic seabirds and marine mammals (Bluhm and Gradinger 2008; Moore and Kuletz 2019), some of which are harvested by subsistence hunters as important food resources.

This environment facilitates efficient sequestration of carbon in sediments and subsurface waters (Wassmann et al. 2004). An estimated 20% of summer primary production, and substantial portions of subsurface dissolved inorganic carbon (DIC), are advected northward into the Arctic basin (Moran et al. 2005; Bates 2006). However, this sequestration is modulated by powerful fall storms that can fully mix the water column and replenish surface waters with remineralized DIC and nutrients (Hauri et al. 2013; Abe et al. 2019). High deposition rates of particulate organic carbon (POC) likely facilitate substantial carbon burial in sediments where total organic carbon (TOC) reaches up to 2% in surface sediments (Grebmeier and McRoy 1988; Grebmeier and Barry 1991).

The tight pelagic-benthic coupling is expected to weaken with climate change due to increased duration of the open-water period for primary production, and resulting declines in total production resulting from nutrient limitation (Piepenburg 2005; Wassmann and Reigstad 2011; Grebmeier 2012). Additionally, warmer waters could increase metabolic rates of pelagic grazers and heterotrophic bacteria, and potentially favor smaller phytoplankton and faster-growing grazers that more rapidly recycle organic matter in the water column (Wassmann and Reigstad 2011).

In 2017 and 2018, the environmental changes on the Pacific Arctic reached unprecedented levels, with bottom waters averaging 3°C warmer than the 2005-2017 baseline and ranking the first and

second lowest maximum Arctic sea-ice extent on record, respectively (Stabeno and Bell 2019). During this period, we observed the strength of the biological carbon pump (BCP) by directly quantifying rates of primary production, sinking POC fluxes, and microbial respiration associated with trap-collected sinking particulate matter. High-resolution imagery of sinking particulate matter was conducted in order to identify the nature and origin of the sinking material. These unique observations provide an opportunity to test current hypotheses regarding the strength of pelagic-benthic coupling, biogeochemical feedbacks, and ecosystem response on Arctic shelves influenced by climate change.

We measured rates of sinking POC flux on the Bering and Chukchi shelves using both moored 24-cup time-series sediment traps (MSTs), and a drifting sediment trap (DST). The DSTs collected short-term flux measurements on the order of several hours in June of 2018. The MST provided an annual time series of flux ranging from 9 to 30 day integrations over the 12 months leading up to our June 2018 expedition. This expedition occurred after the winter with the lowest sea ice extent on record, when the peak ice extent covered only our most northern stations (CL1 and CL3, Figure1). Sea ice had just retreated from these stations when our expedition began.

Overall, sinking POC fluxes were high, reaching 2.2 g C m^{-2} d^{-1}, but spatially variable (Table S1, Figure 1). As predicted by Grebmeier and McRoy (1989), nutrient-rich Bering Shelf/Anadyr Waters (BSAW) was associated with higher fluxes ranging from 1.2 to 2.2 g C m^{-2} d^{-1} at stations CBE1, DBO2.4, and DBO3.8, while lower fluxes ranging from 0.2 to 0.5 g C m^{-2} d^{-1} were characteristic of lower nutrient, fresher Alaska Coastal Waters (ACW) at stations IL4, DBO3.3, and CL1 (Figure 1, Figure S2). For stations in the BSAW, sinking particles consisted mostly of aggregated diatoms and viable diatom cells while more diverse particles including fecal pellets, grazers, and diatom cells were typical of ACW stations (Figure S4).

The two MSTs deployed for a full year immediately prior to our June 2018 DST sampling provide temporal context and independent measures of the extraordinary fluxes that occurred in 2017 and 2018 on the Pacific Arctic shelf. The highest MST fluxes were recorded in June and/or July of these years, and the magnitudes of these fluxes are similar to those measured with the DST method (Table S2, Table S3, Figure S1). The last 8-day integrated measurements of flux from the MSTs finished 3 and 6 days before the deployment of the DST at DBO2.4 and DBO3.8, respectively. We measured fluxes of 831.2 mg C m^{-2} d^{-1} and 1180+/-100 mg C m^{-2} d^{-1} at DBO2.4 and 2291.6 mg C m^{-2} d^{-1} and 1390+/-70 mg C m^{-2} d^{-1} at DBO3.8 for the MST and DST, respectively (Figure 2). Comparable flux magnitudes from these two different methods minimize the concerns over collection biases common with water sediment traps, especially in shallow regions with fast currents (Buesseler et al. 2007). The MST time series indicates that peak vernal flux had passed in the southern stations before DST sampling in early June 2018, but the stations north of Bering Strait appear to be at or near their peak annual flux.

Sinking fluxes were similar to rates of depth-integrated primary productivity, indicating a highly efficient BCP. Export ratios (e-ratios: flux divided by primary productivity) ranged from 0.46 +/- 0.04 to 1.36 +/- 0.12 (Table S4, Figure 2), significantly higher than the typical coastal e-ratio of 0.25 and open-ocean e-ratio of 0.10 (Dunne et al. 2007), but not unprecedented for this region (Moran et al. 2012; Baumann et al. 2013). Generally, higher flux was recorded in areas of higher productivity, with some exceptions. Three stations (DBO2.4, CL3, and IL4) had e-ratios at or above 1 (Figure 2), which can result from relatively high instantaneous fluxes and temporal or spatial decoupling between primary production and flux. Although individual measurements of e-ratios approaching 1 are somewhat common (Moran et al. 2012; Baumann et al. 2013; Le Moigne et al. 2013), our average regional e-ratio of 0.82+/-0.32 (mean +/- 1 S.D.) appears to be unprecedented in the literature as a regional average, further illustrating the exceptional efficiency of the BCP in the Pacific Arctic.

We compared the primary production rates, sinking flux, as well as export ratios from this study with other prior measurements from this study area (Fukuchi et al. 1993; Moran et al. 1997), the broader shelf system (Moran et al. 2005; Baumann et al. 2013), and from a global compilation (Le Moigne et al. 2013) (Figure 2, Figure S5). The primary production rates and e-ratios from this study fall within the same range as those reported previously from the broader Pacific-Arctic shelf system and globally. Our flux measurements, however, are much higher than previous measurements from this study region, the surrounding shelf system, and global values. In fact, the flux measurements from the BSAW sites (CBE1, DBO2.4, and DBO3.8) are higher than all other flux measurements in the regional and global datasets considered here. With only one measurement pair of flux and primary production from this study region previously reported, it is not possible to determine how these values may be different than those in earlier, colder, and ice-replete years. We can, however, establish that the fluxes we measured on the Pacific Arctic shelf in June 2017 and 2018 are amongst the strongest flux events ever observed in this region and the global oceans.

Bacterial production in Arctic waters might increase under more acidic, warmer, and lower-ice conditions (Garneau et al. 2008; Vaqué et al. 2019), which could result in higher community carbon demand (Sala et al. 2010). However, our direct measurements of microbial respiration rates associated with sinking particles were very low, essentially indistinguishable from zero (Table S5, Figure S3). This is not unprecedented in high latitude regions (McDonnell et al. 2015; Belcher et al. 2016). At five of the seven stations there was no significant difference between the control and the experimental respiration rates. On average, the rate of particle-associated microbial respiration was 2 +/- 8% day^{-1}, with a 95% confidence interval ranging from -24.2 to 34.3% day^{-1}. Here, negative carbon-specific rates indicate net respiration or decomposition of POC, while positive rates indicate net production of organic matter, possibly due to viable photosynthetic cells amongst the sinking material. Given the shallow nature of the Pacific Arctic shelf, the low particle associated microbial respiration rates, and likely rapid sinking

velocity of material caught in the traps, we estimate that no more than 10% of the exported organic carbon is being remineralized within the water column before being deposited on the sediments. The true consumption is likely much smaller than this value. We conclude that particle-associated microbial respiration does not play a large role in recycling POC below the euphotic zone in this region in June during a warm, low-ice year. With the combination of negligible particle associated respiration rates and highly efficient e-ratios, we can also infer extremely low levels of organic matter recycling within the euphotic zone.

There is much uncertainty surrounding the effects and feedbacks that will emerge from the rapid environmental changes occurring on the high latitude shelf systems. Our observations of primary production, sinking particle fluxes, and the microbial respiration rates associated with sinking particulate matter indicate that the strength and efficiency of the biological carbon pump of the Pacific Arctic shelf is exceptionally strong amidst a pronounced multi-year shift to warmer and relatively ice-free conditions. Unfortunately, a general lack of historical flux measurements in this region, especially during the late spring bloom, limits our ability to evaluate how these important ecological and biogeochemical fluxes may have changed over time. Moreover, measurements in June may not show zooplankton's response to a shift in environmental conditions as well as measurements in the Fall or Winter. Nonetheless, our observations do not support the predominant hypothesis that a weaker biological carbon pump and stronger pelagic heterotrophy will prevail on the Arctic's continental shelves under future change (Piepenburg 2005; Wassmann and Reigstad 2011; Grebmeier 2012). Instead, we anticipate that this system may retain strong coupling between the pelagic and benthic realms, continue to support highly productive pelagic and benthic ecosystems, and act as a strong sink for atmospheric carbon dioxide. If these results prove to be applicable to other Arctic shelf systems undergoing conditions of sustained warming and loss of sea ice, then these processes could represent an important feature of resilience in regional ecosystems, biogeochemical cycles, and climate.

2.3 Acknowledgements

We would like to thank S. B. Moran for donating materials to this project and the Alaska Stable Isotope Facility for technical support and analytical assistance (University of Alaska, Fairbanks). Many thanks to the Captain and crew of the R/V Sikuliaq. Funded by the NPRB (Grant G-11255 and G-12333 to S.L. Danielson, A. Blanchard, S. Hardy, R.R. Hopcroft, A.M.P. McDonnell, and D. Stockwell).

2.4 References

Abe H, Sampei M, Hirawake T, et al. (2019) Sediment-associated phytoplankton release from the seafloor in response to wind-induced barotropic currents in the Bering Strait. Front Mar Sci 6:1–9. https://doi.org/10.3389/fmars.2019.00097

Bates NR (2006) Air-sea CO_2 fluxes and the continental shelf pump of carbon in the Chukchi Sea adjacent to the Arctic Ocean. J Geophys Res Ocean 111:1–21. https://doi.org/10.1029/2005JC003083

Baumann MS, Moran SB, Lomas MW, et al. (2013) Seasonal decoupling of particulate organic carbon export and net primary production in relation to sea-ice at the shelf break of the eastern Bering Sea: Implications for off-shelf carbon export. J Geophys Res Ocean 118:5504–5522. https://doi.org/10.1002/jgrc.20366

Belcher A, Iversen M, Manno C, et al. (2016) The role of particle associated microbes in remineralization of fecal pellets in the upper mesopelagic of the Scotia Sea, Antarctica. Limnol Oceanogr 61:1049–1064. https://doi.org/10.1002/lno.10269

Bluhm BA, Gradinger RR (2008) Regional Variability in Food Availability. Ecol Appl 18:S77–S96. https://doi.org/http://dx.doi.org/10.1890/06-0562.1

Buesseler KO, Chen M, Harada K, et al. (2007) An assessment of the use of sediment traps for estimating upper ocean particle fluxes. J Mar Res 65:345–416. https://doi.org/10.1357/002224007781567621

Chen L, Gao Z, Sun H, et al. (2014) Distributions and air-sea fluxes of CO_2 in the summer Bering Sea. Acta Oceanol Sin 33:1–8. https://doi.org/10.1007/s13131-014-0483-9

Danielson SL, Eisner L, Ladd C, et al. (2017) A comparison between late summer 2012 and 2013 water masses, macronutrients, and phytoplankton standing crops in the northern Bering and Chukchi Seas. Deep-Sea Res II 135:7–26. https://doi.org/10.1016/j.dsr2.2016.05.024

Dunne JP, Sarmiento JL, Gnanadesikan A (2007) A synthesis of global particle export from the surface ocean and cycling through the ocean interior and on the seafloor. Global Biogeochem Cycles 21:1–16. https://doi.org/10.1029/2006GB002907

Fukuchi M, Sasaki H, Hattori H, et al. (1993) Temporal variability of particulate flux in the northern Bering Sea. Cont Shelf Res 13:693–704. https://doi.org/10.1016/0278-4343(93)90100-C

Garneau MÈ, Vincent WF, Terrado R, Lovejoy C (2009) Importance of particle-associated bacterial heterotrophy in a coastal Arctic ecosystem. J Mar Syst 75:185–197 . http://doi.org/10.1016/j.jmarsys.2008.09.002

Gradinger R (1999) Vertical fine structure of the biomass and composition of algal communities in Arctic pack ice. Mar Biol 133:745–754. https://doi.org/10.1007/s002270050516

Gradinger R (2009) Sea-ice algae: Major contributors to primary production and algal biomass in the Chukchi and Beaufort Seas during May/June 2002. Deep Res Part II Top Stud Oceanogr 56:1201–1212. https://doi.org/10.1016/j.dsr2.2008.10.016

Grebmeier JM (2012) Shifting patterns of life in the Pacific Arctic and Sub-Arctic Seas. Ann Rev Mar Sci 4:63–78. https://doi.org/10.1146/annurev-marine-120710-100926

Grebmeier JM, Barry JP (1991) The influence of oceanographic processes on pelagic-benthic coupling in polar regions : A benthic perspective. J Mar Syst 2:495–518

Grebmeier JM, McRoy CP (1988) Pelagic-benthic coupling on the shelf of the northern Bering and Chukchi Seas. I. Food supply and source and benthic biomass. Mar Ecol Prog Ser 48:57–67. https://doi.org/10.3354/meps053079

Grebmeier JM, McRoy CP (1989) Pelagic-benthic coupling on the shelf of the northern Bering and Chukchi Seas. III. Benthic food supply and carbon cycling. Mar Ecol Prog Ser 53:93–100. https://doi.org/0171-8630/89/0053/0079/$ 03.00

Hauri C, Winsor P, Juranek LW, et al. (2013) Wind-driven mixing causes a reduction in the strength of the continental shelf carbon pump in the Chukchi Sea. Geophys Res Lett 40:5932–5936. https://doi.org/10.1002/2013GL058267

Le Moigne FAC, Henson SA, Sanders RJ, Madsen E (2013) Global database of surface ocean particulate organic carbon export fluxes diagnosed from the ^{234}Th technique. Earth Syst Sci Data 5:295–304. https://doi.org/10.5194/essd-5-295-2013

McDonnell AMP, Boyd PW, Buesseler KO (2015) Effects of sinking velocities and microbial respiration rates on the attenuation of particulate carbon fluxes through the mesopelagic zone. Global Biogeochem Cycles 29:175–193. https://doi.org/10.1002/2014GB004935.

Moore SE, Kuletz KJ (2019) Marine birds and mammals as ecosystem sentinels in and near Distributed Biological Observatory regions: An abbreviated review of published accounts and recommendations for integration to ocean observatories. Deep-Sea Res II 162:211–217. https://doi.org/10.1016/j.dsr2.2018.09.004

Moran SB, Ellis KM, Smith JN (1997) ^{234}Th/^{238}U disequilibrium in the central Arctic Ocean: Implications for particulate organic carbon export. Deep-Sea Res II 44:1593–1606. https://doi.org/10.1016/S0967-0645(97)00049-0

Moran SB, Kelly RP, Hagstrom K, et al. (2005) Seasonal changes in POC export flux in the Chukchi Sea and implications for water column-benthic coupling in Arctic shelves. Deep-Sea Res II 52:3427–3451. https://doi.org/10.1016/j.dsr2.2005.09.011

Moran SB, Kelly RP, Iken K, et al. (2012) Seasonal succession of net primary productivity, particulate organic carbon export, and autotrophic community composition in the eastern Bering Sea. Deep-Sea Res II 65–70:84–97. https://doi.org/10.1016/j.dsr2.2012.02.011

Osborne E, Richter-Menge J, Jeffries M (2018) Arctic Report Card 2018, https://www.arctic.noaa.gov/Report-Card

Piepenburg D (2005) Recent research on Arctic benthos: Common notions need to be revised. Polar Biol 28:733–755. https://doi.org/10.1007/s00300-005-0013-5

Pipko II, Semiletov IP, Tishchenko PY, et al. (2002) Carbonate chemistry dynamics in Bering Strait and the Chukchi Sea. Prog Oceanogr 55:77–94. https://doi.org/10.1016/S0079-6611(02)00071-X

Sala MM, Arrieta JM, Boras JA, et al. (2010) The impact of ice melting on bacterioplankton in the Arctic Ocean. Polar Biol 33:1683–1694 . doi: 10.1007/s00300-010-0808-x

Springer AM, McRoy CP (1993) The paradox of pelagic food webs in the northern Bering Sea-III. Patterns of primary production. Cont Shelf Res 13:575–599. https://doi.org/10.1016/0278-4343(93)90095-F

Stabeno PJ, Bell SW (2019) Extreme Conditions in the Bering Sea (2017–2018): Record-Breaking Low Sea-Ice Extent. Geophys Res Lett 46:8952–8959. https://doi.org/10.1029/2019gl083816

Vaqué D, Lara E, Arrieta JM, et al. (2019) Warming and CO_2 enhance arctic heterotrophic microbial activity. Front Microbiol 10:1-13. https://doi.org/10.3389/fmicb.2019.00494

Vaughan DG, Comiso JC, Allison I, et al. (2013) Observations: Cryosphere. Climate Change 2013 Physical Science Basis. Contribution of Working Group I to the Fifth Assessment Report of the Intergovernmental Panel on Climate Change. 317–382. https://doi.org/10.1017/CBO9781107415324.012

Walsh JJ, McRoy CP, Coachman LK, et al. (1989) Carbon and nitrogen cycling within the Bering/Chukchi Seas: Source regions for organic matter effecting AOU demands of the Arctic Ocean. Prog Oceanogr 22:277–359. https://doi.org/10.1016/0079-6611(89)90006-2

Wassmann P, Bauerfeind E, Fortier M, et al. (2004) Particulate organic carbon flux to the Arctic Ocean sea floor. The organic carbon cycles in the Arctic Ocean. Springer, Berlin, Heidelberg, 101–138. https://doi.org/10.1007/978-3-642-18912-8_5

Wassmann P, Reigstad M (2011) Future arctic Ocean seasonal ice Zones and implications for pelagic-benthic coupling. Oceanography 24:220–231

2.5 Figures

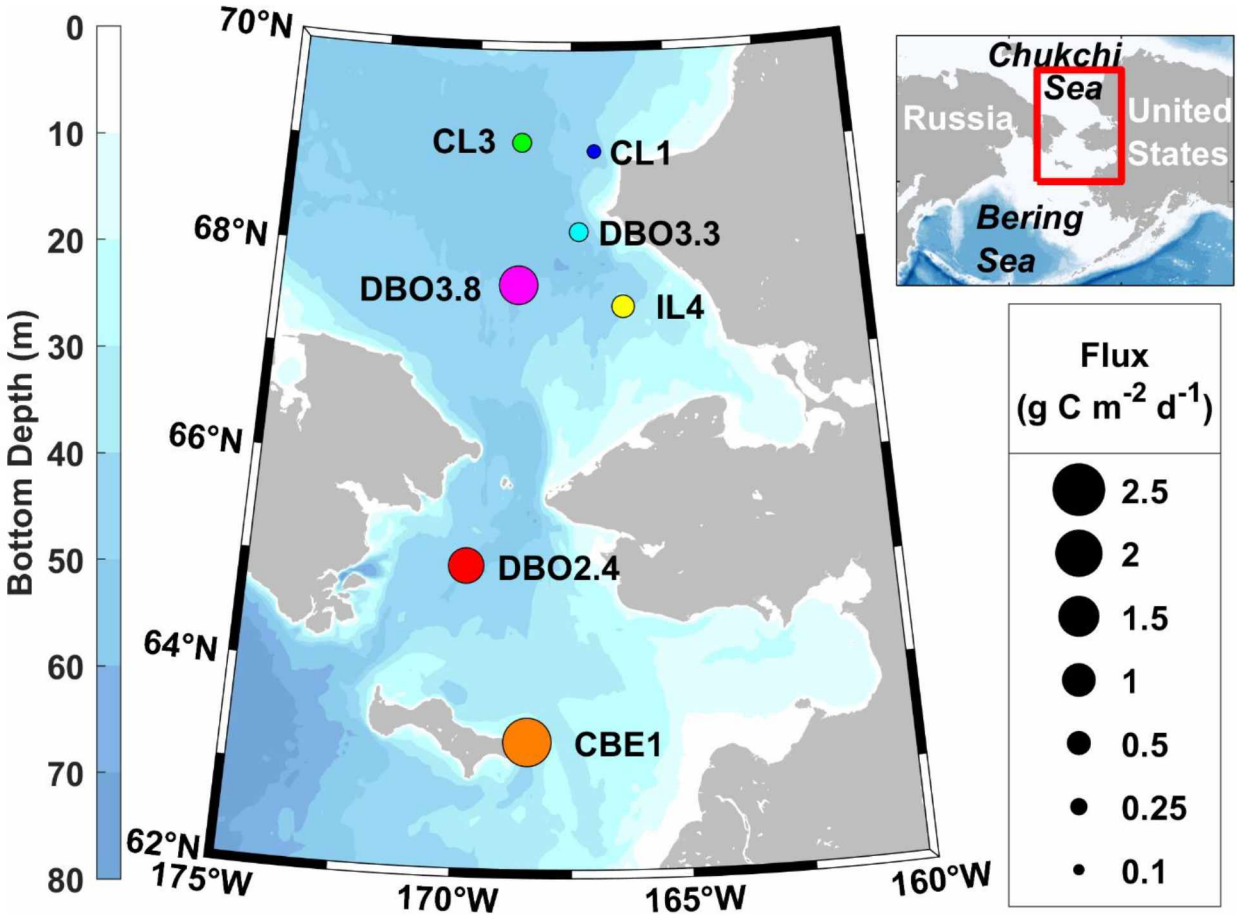

Figure 2.1. Spatial distribution of sinking particulate organic carbon fluxes. Map of the spatial patterns of sinking particulate organic carbon fluxes measured by the DSTs in June 2018. MSTs were deployed adjacent to DBO2.4 (N4) and DBO3.8 (N6).

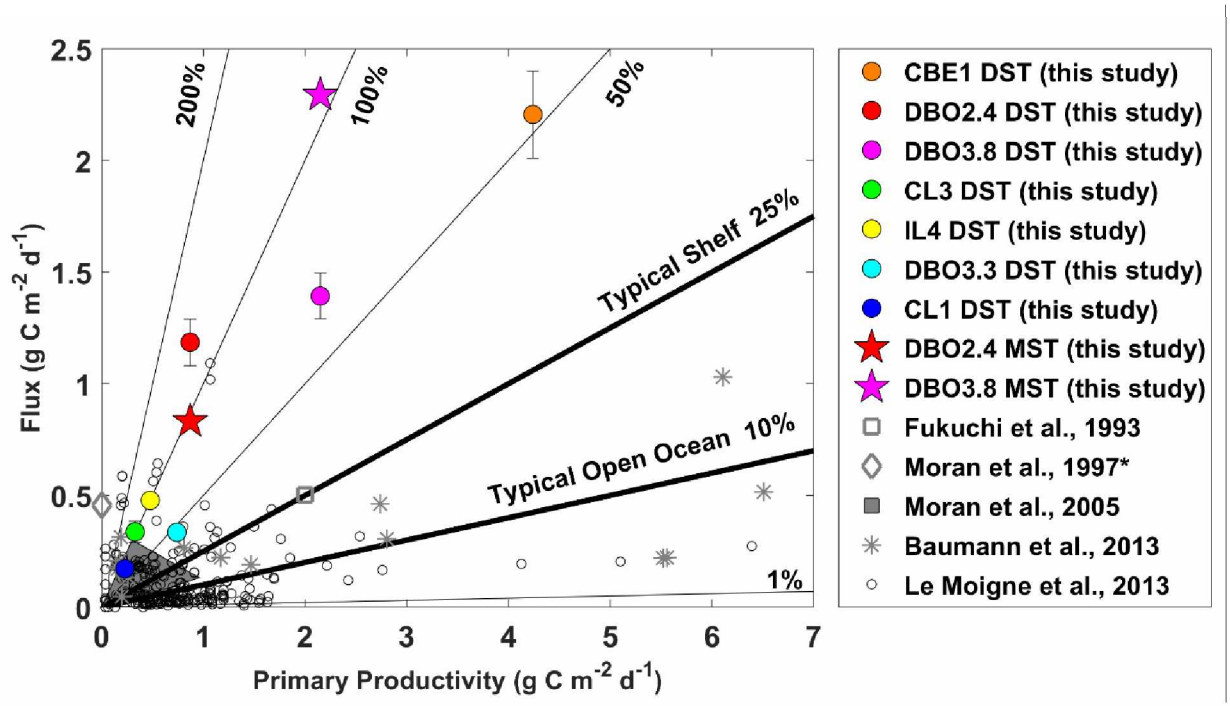

Figure 2.2. Comparison of export efficiency. Rates of flux and primary productivity (PP) with contours of the export ratio (e-ratio) measured in June 2018 on the Pacific Arctic shelf. The stars represent the final flux measurement from the MSTs (9 days of integrated flux) collected immediately prior to recovery of the MST and the deployment of the DST (values plotted against the same PP rates). Grey markers provide regional and global context[2] (Fukuchi et al. 1993; Moran et al. 1997; Baumann et al. 2013; Le Moigne et al. 2013).

[2] No corresponding productivity data with Moran et al., 1997

APPENDIX A

Supporting Online Material for: "Extraordinary carbon fluxes associated with warming and sea ice loss on the Pacific Arctic shelf"

A.1 Materials and Methods

A.1.1 Moored sediment trap sampling

Two 24-cup Hydrobios moored sediment traps were deployed at stations N4 just south of Bering Strait and N6 just north of Bering Strait during the ASGARD cruise in June 2017 (Table S1). The cups were filled with a hyper-saline (salinity 38) 1.85% formalin solution in filtered seawater to reduce the likelihood of flushing, and to prevent biological remineralization of organic matter associated with sinking particles. A carousel rotated on a preprogramed schedule throughout the year, placing one cup under a collection funnel at a time for between seven and forty days (Table S2). Ballast weight below and buoyant floats above ensure upright orientation of the traps throughout the year.

The moored sediment traps were recovered on the subsequent ASGARD cruise in June of 2018. The trap at N4 was recovered earlier than planned, and the 24th cup was still open upon the mooring's recovery. Material that had been collected in that cup was likely disturbed during recovery and therefore was excluded from analysis. The carousel on the trap at station N6 had rotated to close all cups before the mooring's recovery, and therefore all 24 cups could be analyzed. After recovery, cups were removed, sealed with screw-top lids, covered with Parafilm, and finally sealed with electrical tape to ensure no leakage during shipment to the Québec-Océan Lab at the Université Laval for further analysis. Flux was calculated by dividing the total carbon mass by the square area of the funnel head, multiplied by the time interval.

There was greater intra-annual variation in particulate organic carbon (POC) flux at the northern station, with the highest fluxes occurring in late June and July, followed by a period of very low flux from

August through October (Figure S1 and Table S3). Fluxes were elevated in November and December, but bottom current velocity taken from a 300 kHz RDI workhorse ADCP on the mooring suggest this material was likely collected following resuspension events, rather than net export of new production (Abe et al. 2019), especially considering how little light was available at this time of year. This conclusion is further supported by the sharp decrease in flux when sea ice encroached in January, preventing wind mixing. Finally, after ice retreat in May, the highest fluxes of the year were measured in early June. The annual cycle of flux was also observed at the southern station, but to a lesser extent as sea ice was not very prominent south of the Strait during this anomalously low ice year. Additionally, larger flux events occurred in August and September at the southern station, potentially the result of fall bloom events. We sampled this region with DSTs from June 7, 2018 – June 24, 2018. Based on the flux time series from the MSTs, it appears that peak vernal flux had passed in the southern stations before we arrived, but the stations north of the Strait appear to be at their peak annual flux during our sampling, or potentially peak vernal flux occurred after our sampling.

Bottom current speeds regularly exceed 20 cm s^{-1}, even during spring periods when sinking POC flux is highest (Figure S1). Current speeds of this magnitude are known to have implications for flux collection efficiency (Buesseler et al., 2007). This should be taken into account when considering flux measurements collected using MSTs.

A.1.2 Drifting sediment trap sampling

A Lagrangian-type surface-tethered drifting sediment trap (DST) (KC Denmark model number 28.200) was used to collect sinking particles. The trap array consisted of four open-topped tubes on beveled hinges. Two of the tubes contained a removable clear-bottomed cup filled with 250 mL of viscous polyacrylamide gel. The cups were fitted with a sloping ramp to funnel all sinking particles into the gel within the cup and prevent particles from settling between the inside of the tube and the outside

of the cup. All four tubes were filled with filtered seawater (0.3 µm) collected in Niskin bottles from the same depth and station at which the DST was deployed. The water was chilled to 0˚C to increase the density of the solution in order to reduce the likelihood of flushing after deployment. The remaining two tubes collected sinking particles in bulk, maintaining in-situ chemistry as much as possible. The DST was carefully deployed to prevent filtrate from spilling out of the tubes. The trap array was deployed at 30 m below the surface, estimated as the bottom of the euphotic zone, for between three and eleven hours depending on the timing of other cruise operations. The actual 1% light level varied from between 16 and 30 m, with only CL3 having a euphotic zone deeper than 30 m where it reached 38 m (Table S4). The DST was fitted with an ARGOS beacon and a go-Tele GPS tracker unit to track its real-time location (Figure S2 and Figure 1, main text).

A.1.3 Respiration and flux rate measurements

Sinking particles collected in the DST were used to determine rates of POC flux. Once the DST was recovered, the following steps were performed as quickly as possible in an environmental chamber set to 0° C in order to maintain as close to *in situ* conditions for particle-associated microbes as possible. Overlying water was siphoned using a vacuum pump until reaching a boundary layer just above where sinking particles had settled towards the bottom of all four tubes. In the two bulk particle collection tubes, the material that remained in the tubes after siphoning was quantitatively split into four subsamples using a Folsom plankton splitter. Three subsamples were used for triplicate analytical flux measurements. These samples were filtered onto precombusted 25-mm Whatman glass fiber filters (GF/F) and placed in a dehydrator at 60 C for 12 hours. Once dry, the filters were sealed in Petri dishes until further analysis.

The remaining subsample from each of the two tubes was used to calculate particle-associated microbial respiration rates. This material was homogenized by swirling the container and pipetted with a wide-bore pipette into 8 replicate 2-mL glass vials (Batch PSTS-1721-01) fitted with Pre-Sens Oxygen

Optode Sensor Spots (Regensburg, Germany) per tube, totaling 16 experimental samples. Filtered seawater controls were obtained from a Niskin bottle closed at 30 m depth during a CTD cast upon recovery of the DST. Water was filtered (0.3 µm) to remove particles and particle-associated microbes. Free-living microbes remained. The filtrate was pipetted into 8 replicate vials that were identical to the experimental vials. All 24 vials were checked for air bubbles, and vials were then placed inside a sealable clear plastic water-bath that was placed on top of a PreSens SDR SensorDish Reader version 4 (Serial Numbers S EBX 0007 000514 and S EBX 0007 000625, Regensburg, Germany). The water-bath was located inside a cold-room that varied from 3-5°C and connected to a Fisherbrand Isotemp 500LCSU 115V/60HZ Cooling/Heating Recirculating Circulator (a.k.a. a chiller), that maintained temperature at precisely 4.0˚C during the incubation. The concentration of oxygen in each vial and temperature in the incubation chamber were recorded every 30 seconds for the duration of the incubation using PreSens - Sensor Dish Reader Version 4 Software.

A few modifications to the methods were made during the course of the study. After the first incubation at CBE1 low-oxygen micro-environments formed around the sensor spot, located at the bottom of the vial. For subsequent incubations, the entire incubation chamber was repeatedly inverted for 5 seconds every 3 minutes to mix the sample. The concentration of oxygen increased over time in a few of the experimental samples, suggesting photosynthetic activity. During the last two incubations at CL1 and CL3, a black cloth was used to cover the incubation chamber in order to prevent any light from reaching the samples, theoretically preventing light reactions associated with photosynthesis. It should be noted that dark reactions associated with photosynthesis can continue for several hours after the removal of light in cold water. Incubations lasted for between 3 and 12 hours. After incubations were completed, the remaining material from each vial was filtered onto individual GF/F filters and treated the same as the flux measurement samples.

The data recorded by the PreSens software were downloaded and analyzed using the following steps in Matlab 2017a computing software. Data collected before the incubation temperature stabilized were trimmed so that only the time during which the incubation temperature remained stable was analyzed. The first hour of data after temperature stabilization was used to determine respiration rates. Linear regression analysis was performed on the data from each vial. The average and standard deviation of the 8 replicate control slopes was taken, and for each of the two experimental samples. Then the average slopes for each of the experimental incubations were averaged together and the error was propagated. The difference between the experimental slope and the control slope is equivalent to the rate of oxygen uptake of particle associated microbes. This rate was converted to units of CO_2 production using a 117:170 carbon to oxygen ratio, which can be assumed to have a one to one relationship with organic carbon degradation (Anderson and Sarmiento 1994) (Figure S3 and Table S5).

A.1.4 Sinking particle visualization

Collecting particles in polyacrylamide gel keeps sinking particles intact and allows for particle identification (Ebersbach and Trull 2008; Buesseler et al. 2010; Durkin et al. 2015). After overlying filtrate was siphoned from the two tubes with cups of polyacrylamide gel, the cups were carefully removed. Remaining overlying water was pipetted off until only gel and sinking particles remained in the cups. The contents of the cups were photographed as quickly as possible using a Sony A7RII 42.4 MP digital mirrorless camera with a Sony FE 50 mm f/2.8 Macro Lens and a Flashpoint Zoom LI-ON R2 flash unit. A length to pixel relationship was determined for each image in Photoshop (Figure S4).

A.1.5 Primary productivity rate measurements

^{13}C-^{15}N dual-isotope tracer technique was used to measure integrated rates of primary productivity at thirteen stations. Seven stations overlapped where measurements of primary productivity, flux, and particle-associated microbial respirations were taken (Table S4). For primary productivity rate measurements, water was collected at 6 depths representing the 100%, 50%, 30%,

12%, 5% and 1% light levels. The 1% light level is estimated to be the minimum amount of light necessary for photosynthesis to occur, or the bottom of the euphotic zone. Samples were collected in triplicate acid-cleaned, screened, 1-L clear polycarbonate bottles and one dark bottle, spiked with $H^{13}CO_3$ and $K^{15}NO_3$, and then covered with a series of screens mimicking *in situ* light levels. Bottles were placed in an incubation chamber and cooled with circulating water on the deck. The incubations lasted for 6 hours, and measurements were extrapolated to daily production by multiplying the rate by 4 given the continuous daylight during this time of year. Incorporation of ^{13}C and ^{15}N into phytoplankton biomass was used to estimate the rate of net primary production. At the end of the experiment, contents in each incubation bottle were filtered onto precombusted GF/F filters and frozen at -20° C until further analysis. Final amount of ^{13}C and ^{15}N is compared with original amount to determine total primary productivity rates. These depth-specific rates are then integrated over the entire depth of the euphotic zone to determine total water column primary productivity rates in units of g organic carbon $m^{-2}\ d^{-1}$.

A.1.6 Elemental POC/PON/^{13}C/^{15}N Analysis

All dried or frozen GF/F filters were processed in the Alaska Stable Isotope Facility at the University of Alaska, Fairbanks. Filters were acidified with 10% hydrochloric acid for 24 hours to remove particulate inorganic carbon (PIC). Filters were peeled to remove separate filter with particulate organic matter (POM) from excess filter, which can clog the elemental analyzer. The peeled filters were pelletized in aluminum cups. Standards of peptone were also prepped and weighed to be run with the samples. All standards and samples were analyzed with a Carbon Nitrogen Elemental Analyzer coupled with an Isotope-Ratio Mass Spectrometer in order to determine the concentration of TOC, TN, $\delta^{13}C$, and $\delta^{15}N$. Standards were run after every 10 samples to ensure no instrument drift.

Flux is measured as grams of organic carbon per meter squared per day (g C $m^{-2}\ d^{-1}$). The average of the three replicate flux measurements from each tube was taken along with the standard deviation of

these values. These values were averaged with the second tube's average flux and then divided by the square area of the opening of the tube (diameter 72 mm, area 0.41m^2) multiplied by the amount of time the trap was deployed (Table S3). One out of six subsamples from IL4 was removed from analysis as an outlier constituting more than 3 standard deviations higher flux than the other subsamples. The error between the tubes was propagated.

A.1.7 Comparing Flux, PP, and E-ratios

Fluxes out of the euphotic zone collected using a DST deployed at 30 m below the sea surface ranged from 172 +/- 10 to 2204 +/- 195 mg C m^{-2} d^{-1}. The upper range of these measurements was unprecedentedly high compared to other measurements in this region, in the surrounding region, and globally (Figure 1, main text and Table S4). Only two previous studies report particulate flux estimates for the Bering and Chukchi shelves, one of which was based on sediment trap measurements. In that study, a moored sediment trap deployed (36 m water depth, 49 m bottom depth) from late June to late September 1988, about 500 miles south of Bering Strait, collected flux measurements ranging from 253 - 654 mg C m^{-2} d^{-1} (Fukuchi et al. 1993). An estimate of 456 mg C m^{-2} d^{-1} (36 water depth, 49 bottom depth) was calculated using the Thorium-234/Uranium-238 disequilibrium method on the Chukchi Sea shelf in August 1994, however no corresponding primary productivity value was measured (Moran et al. 1997). We plotted this flux measurement directly on the y-axis indicating no known primary productivity value (Figure 2, main text). Flux has been estimated more frequently on the Bering and Chukchi shelf breaks, with a maximum value of 3278 mg C m^{-2} d^{-1} reported slightly south of our study area on the Bering Sea shelf break (25 m water depth, >125 m bottom depth) during May 2009 (Baumann et al. 2013) (Figure S5). While this value is higher than our measurements, our average regional flux, 872 +/- 749 mg C m^{-2} d^{-1}, calculated as the mean of all flux measurements +/- 1 standard deviation (Table S4), is much higher than previous average regional flux estimates from the shelf breaks just north and south of this region, which range from 34 +/- 63.7 to 240 +/- 174 mg C m^{-2} d^{-1} (Moran et al. 2005, 2012; Lepore et

al. 2007; Baumann et al. 2013). The only reported fluxes from outside the Bering and Chukchi seas that surpass our estimates were measured in the Baltic Sea, reaching 2500 mg C m^{-2} d^{-1} (Gustafsson et al. 2013). Le Moigne et al. (Le Moigne et al. 2013) conducted a review of global flux calculations using the thorium disequilibrium method (Figure 2, main text). Three of our stations in BSAW rank higher than any of the flux measurements from this study with corresponding PP values. With individual values of flux as well as an average regional flux ranking among the highest ever recorded, this region clearly exports massive amounts of organic carbon out of the euphotic zone, even in an anomalously warm year. Export ratios were calculated using Equation 2.

$$e-ratio = \frac{Flux}{PP} * 100\% \qquad \textit{Equation 2}$$

A.2 Environmental Conditions

During the ASGARD expedition in June of 2018, sea surface temperatures ranged from 1˚C to 10˚C with the warmest water above 8˚C appearing south of Nome and west of Norton Sound. These waters were characteristically fresher, with salinities ranging from 30 to 30.5, consistent with Alaska Coastal Water (ACW) characteristics and a shift to wind direction from the south. During the cruise, wind generally came from the North. Wind speed ranged from 0 to 36 kt during the course of the cruise. Throughout the water column, temperatures ranged from -0.5˚C to 10˚C and salinities ranged from 30 to 33.5. Chlorophyll fluorescence ranged from 0 – 15 µg/L and nitrate concentration ranged from 0 to 20 umol/L, and were at highest concentrations during the cruise along the most northern Cape Lisburne line at the surface and bottom, respectively. No sea ice was observed during the cruise.

A.3 References

Abe H, Sampei M, Hirawake T, et al. (2019) Sediment-associated phytoplankton release from the seafloor in response to wind-induced barotropic currents in the Bering Strait. Front Mar Sci 6:1–9. https://doi.org/10.3389/fmars.2019.00097

Anderson LA, Sarmiento JL (1994) Redfield ratios of remineralization determined by nutrient data analysis. Global Biogeochem Cycles 8:65–80. https://doi.org/10.1029/93GB03318

Baumann MS, Moran SB, Lomas MW, et al (2013) Seasonal decoupling of particulate organic carbon export and net primary production in relation to sea-ice at the shelf break of the eastern Bering Sea: Implications for off-shelf carbon export. J Geophys Res Ocean 118:5504–5522. https://doi.org/10.1002/jgrc.20366

Buesseler KO, Chen M, Harada K, et al (2007) An assessment of the use of sediment traps for estimating upper ocean particle fluxes. J Mar Res 65:345–416. https://doi.org/10.1357/002224007781567621

Buesseler KO, McDonnell AMP, Schofield OME, et al (2010) High particle export over the continental shelf of the west Antarctic Peninsula. Geophys Res Lett 37:1–5. https://doi.org/10.1029/2010GL045448

Durkin CA, Estapa ML, Buesseler KO (2015) Observations of carbon export by small sinking particles in the upper mesopelagic. Mar Chem 175:72–81. https://doi.org/10.1016/j.marchem.2015.02.011

Ebersbach F, Trull TW (2008) Sinking particle properties from polyacrylamide gels during the KErguelen Ocean and Plateau compared Study (KEOPS): Zooplankton control of carbon export in an area of persistent natural iron inputs in the Southern Ocean. Limnol Oceanogr 53:212–224. https://doi.org/10.4319/lo.2008.53.1.0212

Fukuchi M, Sasaki H, Hattori H, et al (1993) Temporal variability of particulate flux in the northern Bering Sea. Cont Shelf Res 13:693–704. https://doi.org/10.1016/0278-4343(93)90100-C

Gustafsson Ö, Larsson U, Andersson P, et al (2013) An assessment of upper ocean carbon and nitrogen export fluxes on the boreal continental shelf: A 3-year study in the open Baltic Sea comparing sediment traps, ^{234}Th proxy, nutrient, and oxygen budgets. Limnol Oceanogr Methods 11:495–510. https://doi.org/10.4319/lom.2013.11.495

Le Moigne FAC, Henson SA, Sanders RJ, Madsen E (2013) Global database of surface ocean particulate organic carbon export fluxes diagnosed from the ^{234}Th technique. Earth Syst Sci Data 5:295–304. https://doi.org/10.5194/essd-5-295-2013

Lepore K, Moran SB, Grebmeier JM, et al (2007) Seasonal and interannual changes in particulate organic carbon export and deposition in the Chukchi Sea. J Geeophys Res 112:1–14. https://doi.org/10.1029/2006JC003555

McDonnell AMP, Boyd PW, Buesseler KO (2015) Effects of sinking velocities and microbial respiration rates on the attenuation of particulate carbon fluxes through the mesopelagic zone. Global Biogeochem Cycles 29:175–193. https://doi.org/10.1002/2014GB004935.Received

Moran SB, Ellis KM, Smith JN (1997) ^{234}Th/^{238}U disequilibrium in the central Arctic Ocean: Implications for particulate organic carbon export. Deep-Sea Res II 44:1593–1606. https://doi.org/10.1016/S0967-0645(97)00049-0

Moran SB, Kelly RP, Hagstrom K, et al (2005) Seasonal changes in POC export flux in the Chukchi Sea and implications for water column-benthic coupling in Arctic shelves. Deep-Sea Res II 52:3427–3451. https://doi.org/10.1016/j.dsr2.2005.09.011

Moran SB, Kelly RP, Iken K, et al (2012) Seasonal succession of net primary productivity, particulate organic carbon export, and autotrophic community composition in the eastern Bering Sea. Deep-Sea Res II 65–70:84–97. https://doi.org/10.1016/j.dsr2.2012.02.011

A.4 Supplemental Tables

Table S1. Location and duration of Drifting Sediment Trap (DST) deployment and recovery. A Lagrangian drifting sediment trap was deployed 7 times for between 3 and 12 hours at 30 m below the sea surface. This trap collects sinking particles as it floats with a water mass.

Station Name	Bottom Depth (m)	Latitude Deploy (Degrees Decimal Minute)	Longitude Deploy (Degrees Decimal Minute)	Latitude Recover (Degrees Decimal Minute)	Longitude Recover (Degrees Decimal Minute)	Date and time of Deployment (M/DD/YYYY HH:MM UTC)	Date and time of Recovery (M/DD/YYYY HH:MM UTC)	Total time of Deployment
CBE1	41	63° 18.1’	-168° 27.0’	63° 12.7’	-168° 25.6’	6/7/2018 15:05	6/8/2018 2:40	11h 35m
DBO2.4	50	64° 58.6’	-169° 52.8’	64° 57.6’	-169° 47.3’	6/11/2018 10:59	6/11/2018 17:29	6h 40m
IL4	42	67° 28.3’	-166° 12.5’	67° 30.9’	-166° 10.5’	6/13/2018 11:57	6/13/2018 20:44	8h 47m
DBO3.8	50	67° 40.4’	-168° 50.1’	67° 41.4’	-168° 51.3’	6/14/2018 23:10	6/15/2018 4:52	5h 42m
DBO3.3	49	68° 11.1’	-167° 18.6’	68° 10.8’	-167° 19.8’	6/15/2018 19:30	6/15/2018 22:55	3h 25m
CL3	51	69° 2.1’	-168° 49.4’	69° 0.5’	-168° 51.4’	6/16/2018 19:41	6/17/2018 0:10	4h 29m
CL1	46	68° 57.3’	-166° 53.8’	68° 54.9’	-166° 53.5’	6/17/2018 21:18	6/18/2018 2:20	5h 2m

Table S2. Location and duration of Moored Sediment Traps (MST). Two MSTs provide a timeline of sinking particles flux from June of 2017 to June of 2018 at two stations.

Trap Name	Date Deployed (UTC)	Date Recovered (UTC)	Trap Depth (m)	Bottom Depth (m)	Latitude (Degrees Decimal Minute)	Longitude (Degrees Decimal Minute)
N4	25-Jun-2017 04:38	11-Jun-2018 14:39	37	49	64° 55. 7’	-169° 55.1’
N6	15-Jun-2017 00:48	15-Jun-2018 03:30	35	50	67° 40.2’	-168° 44.7’

Table S3. Annual time series of flux from Moored Sediment Traps.

Trap Name	Bottle Number	Date Open	Date Close	Duration (Days)	Flux (g C m^{-2} d^{-1})	Trap Name	Bottle Number	Date Open	Date Close	Duration (Days)	Flux (g C m^{-2} d^{-1})
N4	1	26-Jun-2017	3-Jul-2017	7	246.2	N6	1	17-Jun-2017	25-Jun-2017	8	1638.0
	2	3-Jul-2017	11-Jul-2017	8	624.5		2	25-Jun-2017	3-Jul-2017	8	1262.5
	3	11-Jul-2017	19-Jul-2017	8	150.0		3	3-Jul-2017	11-Jul-2017	8	1725.1
	4	19-Jul-2017	27-Jul-2017	8	195.1		4	11-Jul-2017	19-Jul-2017	8	293.3
	5	27-Jul-2017	4-Aug-2017	8	95.0		5	19-Jul-2017	27-Jul-2017	8	355.9
	6	4-Aug-2017	12-Aug-2017	8	159.6		6	27-Jul-2017	4-Aug-2017	8	412.6
	7	12-Aug-2017	20-Aug-2017	8	1228.6		7	4-Aug-2017	12-Aug-2017	8	184.2
	8	20-Aug-2017	28-Aug-2017	8	84.7		8	12-Aug-2017	20-Aug-2017	8	235.6
	9	28-Aug-2017	5-Sep-2017	8	684.7		9	20-Aug-2017	28-Aug-2017	8	366.5
	10	5-Sep-2017	13-Sep-2017	8	69.3		10	28-Aug-2017	5-Sep-2017	8	66.4
	11	13-Sep-2017	21-Sep-2017	8	55.3		11	5-Sep-2017	13-Sep-2017	8	77.5
	12	21-Sep-2017	29-Sep-2017	8	83.8		12	13-Sep-2017	21-Sep-2017	8	344.0
	13	29-Sep-2017	7-Oct-2017	8	55.7		13	21-Sep-2017	29-Sep-2017	8	195.0
	14	7-Oct-2017	15-Oct-2017	8	66.7		14	29-Sep-2017	7-Oct-2017	8	194.2
	15	15-Oct-2017	31-Oct-2017	16	65.2		15	7-Oct-2017	15-Oct-2017	8	336.1
	16	31-Oct-2017	2-Dec-2017	32	1399.0		16	15-Oct-2017	31-Oct-2017	16	485.5
	17	2-Dec-2017	11-Jan-2018	40	979.3		17	31-Oct-2017	2-Dec-2017	32	919.7
	18	11-Jan-2018	20-Feb-2018	40	490.1		18	2-Dec-2017	11-Jan-2018	40	1240.4
	19	20-Feb-2018	1-Apr-2018	40	646.4		19	11-Jan-2018	20-Feb-2018	40	236.4
	20	1-Apr-2018	3-May-2018	32	339.8		20	20-Feb-2018	1-Apr-2018	40	152.0
	21	3-May-2018	23-May-2018	20	183.8		21	1-Apr-2018	3-May-2018	32	468.2
	22	23-May-2018	31-May-2018	8	1476.6		22	3-May-2018	23-May-2018	20	323.2
	23	31-May-2018	8-Jun-2018	8	831.2		23	23-May-2018	31-May-2018	8	706.5
	24	8-Jun-2018	16-Jun-2018	8*	-		24	31-May-2018	8-Jun-2018	8	2291.6

*Cup was open upon collection. POC contents were not analyzed.

Table S4. Flux, primary productivity, and export ratios at 7 stations in the Bering and Chukchi seas at Drifting Sediment Trap (DST) sites.

Station Name	Bottom Depth (m)	Euphotic Zone Depth (m)	Flux (g C m^{-2} d^{-1})	Primary Productivity (g C m^{-2} d^{-1})	Export Ratio
CBE1	41	16	2.20 +/- 0.19	4.24	0.52 +/-0.0 5
DBO2.4	50	24	1.18 +/- 0.10	0.87	1.36 +/- 0.12
IL4	42	26	0.48 +/- 0.03**	0.48	1.00 +/- 0.07
DBO3.8	50	24	1.39+/- 0.07	2.15	0.65 +/- 0.05
DBO3.3	49	30	0.34 +/- 0.03	0.74	0.45 +/- 0.04
CL3	51	38*	0.34 +/- 0.05	0.33	1.02 +/- 0.14
CL1	46	24	0.17 +/- 0.00	0.23	0.75 +/- 0.06

*Euphotic zone depth deeper than 30 m, the depth of the Drifting Sediment Trap (DST) deployment.

** Outlier of 3 standard deviations higher than other 3 replicates removed from analysis

Table S5. Particle-associated microbial respiration rates and carbon specific rates for sinking material. Significant rates in bold and italicized. A total of 189 minutes were analyzed treating all 16 experimental sample as replicates and the final carbon value used to calculate the per carbon rate.

Station Name	r_exp (μmol O_2 m^{-1} L^{-1})	r_control (μmol O_2 m^{-1} L^{-1})	r_PAM (μmol O_2 m^{-1} L^{-1})	R_PAM (% day^{-1})
CBE1	-0.215+/-0.120	-0.076+/-0.086	-0.139+/-0.147	10.3+/-24.0
DBO2.4	***-0.073+/-0.070***	0.017+/-0.018	***-0.090+/-0.072***	***-13.7+/-10.5***
IL4	0.048+/-0.024	***0.030+/-0.012***	0.018+/-0.027	-0.9+/-5.7
DBO3.8	***0.087+/-0.044***	-0.001+/-0.009	***0.088+/-0.045***	***12.8+/-6.7***
DBO3.3	0.019+/-0.032	-0.001+/-0.010	0.020+/-0.033	4.3+/-8.0
CL3	0.007+/-0.041	***-0.009+/-0.008***	0.016+/-0.042	4.2+/-9.5
CL1	-0.008+/-0.032	-0.003+/-0.008	-0.005+/-0.033	-0.8+/-7.5

A.5 Figures

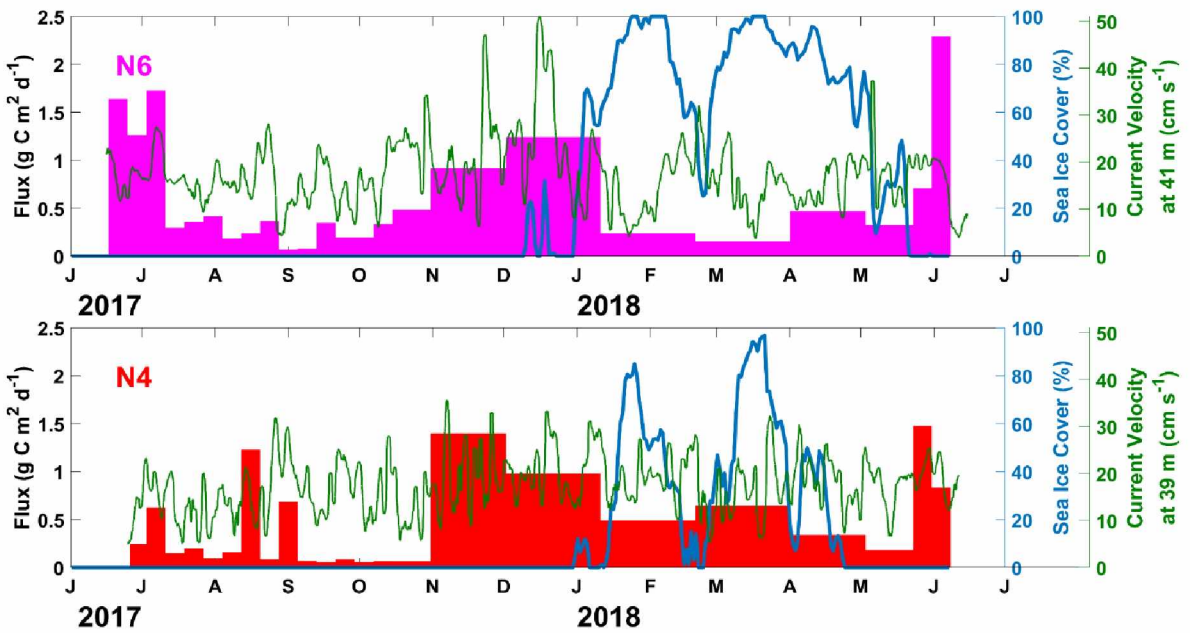

Figure S1. Time series of sinking particulate organic carbon flux. Particulate organic carbon flux (colored bars) measured with moored sediment traps at stations N6 (a) and N4 (b).

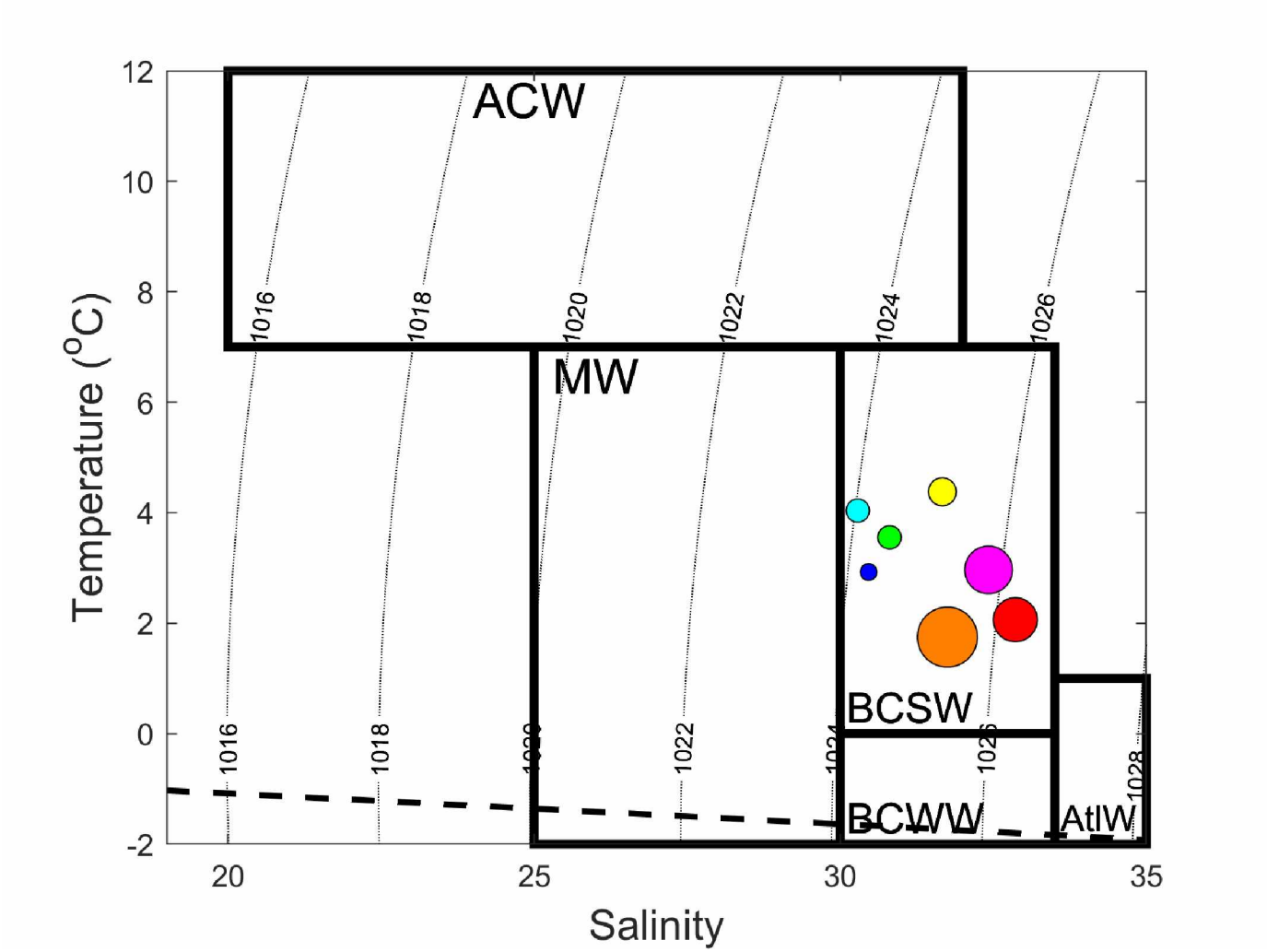

Figure S2. Water mass characteristics at drifting sediment trap stations. The size of the circle is indicative of the amount of organic carbon flux. Water masses are defined as follows: Atlantic Water (AtlW), Bering/Chukchi Winter Water (BCWW), Bering/Chukchi Shelf Water (BCSW), Melt Water (MW), and Alaskan Coastal Water (ACW).

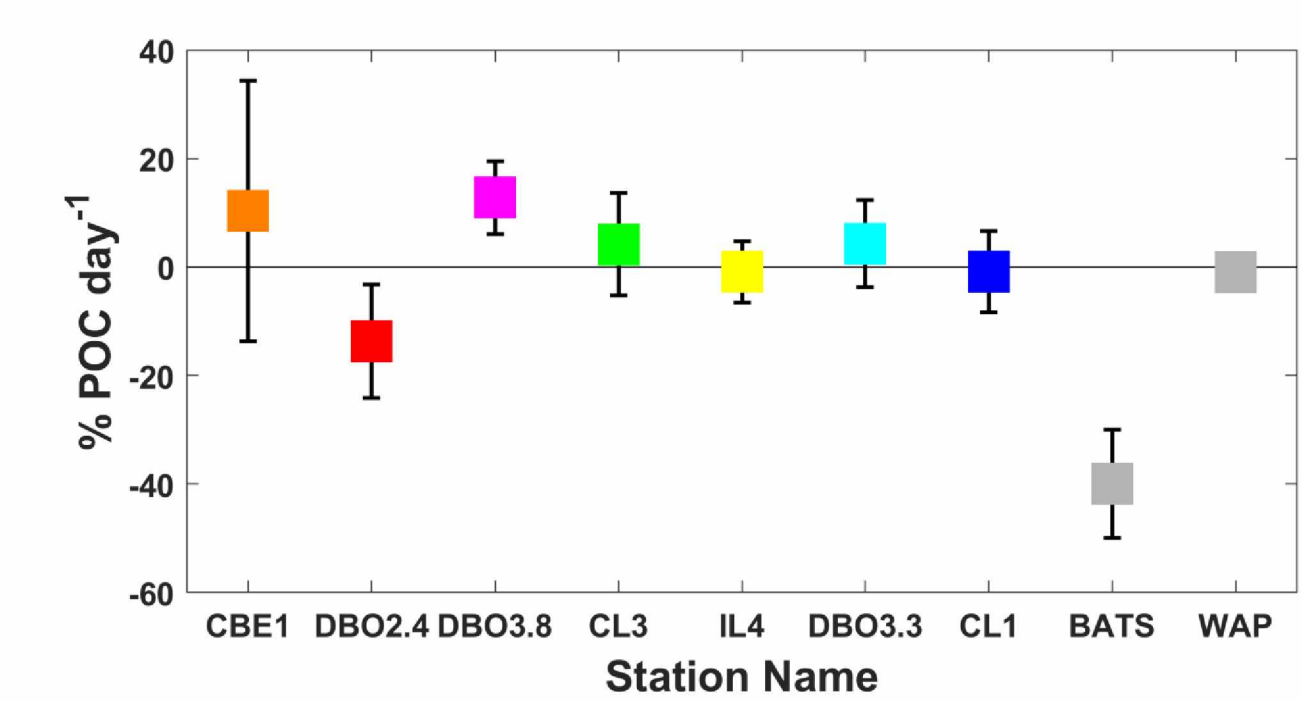

Figure S3. Comparison of particle associated microbial respiration rates. Visualization of particle associated microbial respiration rates from this study along with two previous measurements at the Bermuda Atlantic Time Series (BATS) and Western Antarctic Peninsula (WAP) from McDonnell et al. (2015).

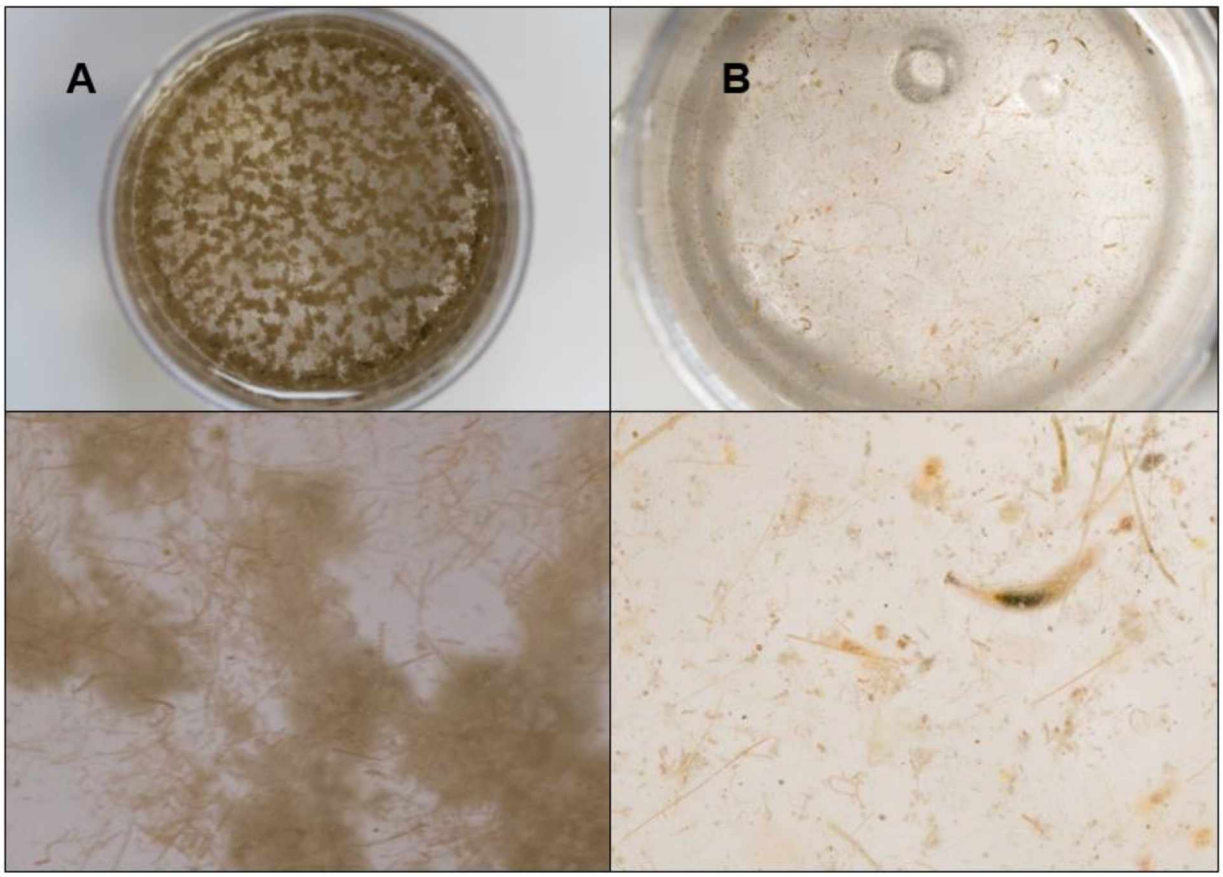

Figure S4. Visualization of sinking particulate material. Images of sinking particles collected in polyacrylamide gel traps at stations CBE1 (Left panels) and IL4 (Right Panels). Lower images show a magnified subsample of the gel above it.

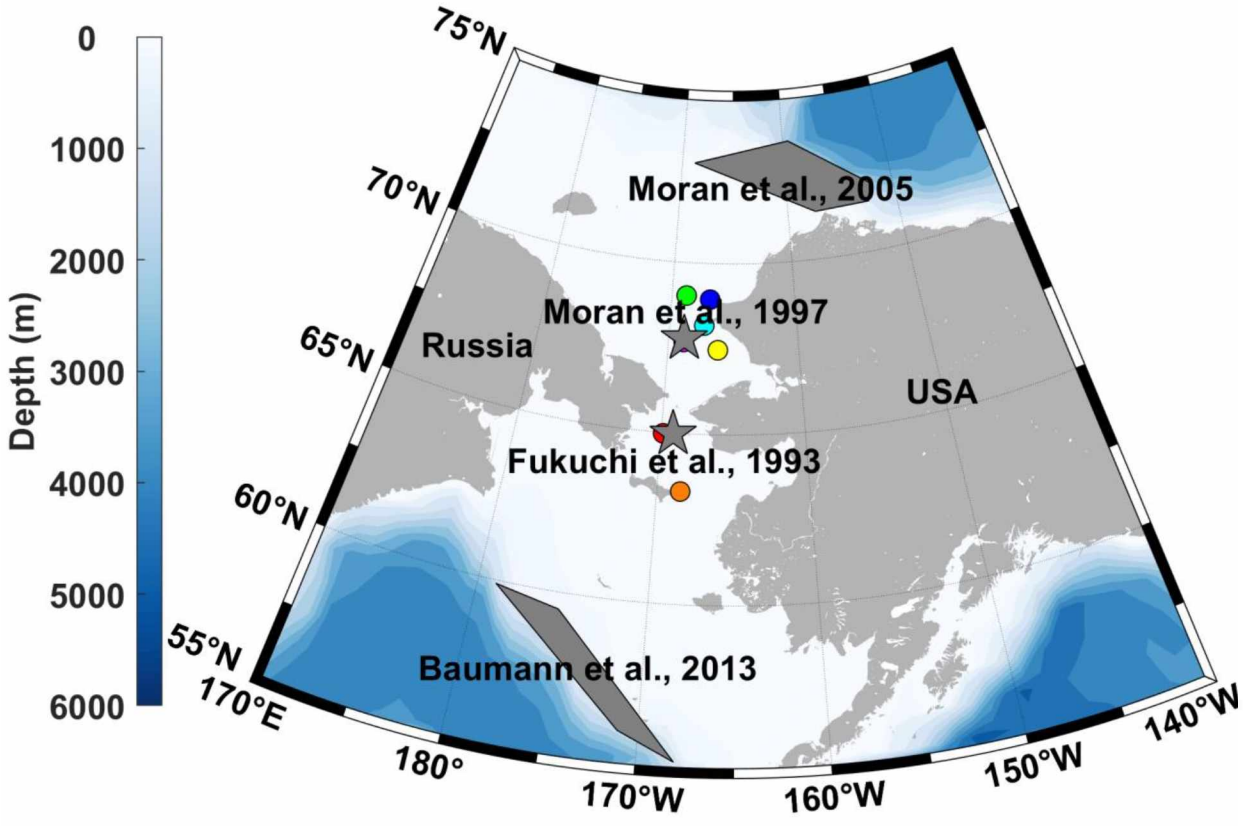

Figure S5. Spatial distribution of sinking particulate organic carbon flux measurements on the Pacific-Arctic shelf. Location of previous carbon flux and primary productivity studies on or near the Bering and Chukchi shelf (grey stars and patches) with location of stations from this study marked with colored circles.

General Conclusion

The connection between the pelagic and benthic zones on the Bering and Chukchi sea shelves is described regularly (Grebmeier and McRoy 1989; Cooper et al. 2012; Grebmeier 2012), but rarely directly measured in this region (Fukuchi et al. 1993; Moran et al. 1997). This goal was achieved by measuring rates of flux of organic carbon out of the euphotic zone and measuring the rate of microbial respiration associated with that sinking material. Furthermore, these measurements were made at an under sampled time of year even though this time of year is thought to be the most important in determining how much energy becomes available to benthic production (Pirtle-Levy et al. 2009).

Amongst the highest rates of sinking particulate organic carbon flux ever recorded in this region and in the global oceans were measured. Additionally, low rates of microbial respiration were measured associated with sinking particles. This pattern of low respiration held true both in BSAW and ACW. These measurements of high flux and low respiration combined are indicative of a strong biological carbon pump or tight pelagic-benthic coupling.

These results do not support the hypothesis of a loosening of pelagic-benthic coupling as predicted for Arctic continental shelves (Piepenburg 2005; Wassmann and Reigstad 2011; Grebmeier 2012). Additionally, respiration measurements do not support the findings of Anderson (1988) that microbial remineralization is more important in ACW than BSAW. My findings bolster the ranking of this region as one of the most important for carbon cycling globally.

We cannot know definitively if flux has increased or decreased on the Bering and Chukchi sea shelves in the early spring because there are so few measurements of flux in this region in general, but especially at this time of year. Continued monitoring of flux will help determine if the rate of organic carbon flux is changing with climate change. This could be accomplished by deploying DSTs in coming years at the same time of year (June), or even earlier as sea ice retreat is occurring earlier than ever (Osborne et al. 2018). The MSTs were redeployed at DBO2.4 and DBO3.8 and will be recovered in the

late summer of 2019. These data should be compared with the results from the first year to see if the general annual pattern of flux is maintained. If not, more MSTs should be deployed to see how annual flux varies year to year. Additionally, no MSTs were deployed in ACW. Having an annual time series of flux from this water mass will also be useful in characterizing flux in this region. However, given the strong current velocities and subsequent resuspension of particles in this region, DST deployment or 234-Thorium disequilibrium method might be better approaches than additional MST deployment to determine flux throughout the year. More remineralization experiments should be done at different times of year. It is likely that later in the summer these rates will be higher than they were in June. If these experiments are repeated, I would suggest a substantial redesign in the methods by using an automatic inverter to help homogenize the sample rather than relying on manual inversion. Care should be taken to ensure the tray and plate reader remain bonded and that the electronics and circulator remain attached during the automatic inversion. These additional studies will help determine how the Arctic's biogeochemical cycling is changing with climate change and will be important for climate modelers to capture accurately in regional and global climate models.

References

Andersen, P (1988) The quantitative importance of the '"microbial loop"' in the marine pelagic: a case study for the North Bering/Chukchi Sea. Arch für Hydrobiol.31, 243–251.

Cooper, LW, Janout, MA, Frey, KE, et al. (2012) The relationship between sea ice break-up, water mass variation, chlorophyll biomass, and sedimentation in the northern Bering Sea. Deep Sea Res II 65–70, 141–162. https://doi.org/10.1016/j.dsr2.2012.02.002

Fukuchi, M, Sasaki, H, Hattori, H, et al. (1993) Temporal variability of particulate flux in the northern Bering Sea. Cont. Shelf Res. 13, 693–704. https://doi.org/10.1016/0278-4343(93)90100-C

Grebmeier, JM (2012) Shifting patterns of life in the Pacific Arctic and Sub-Arctic seas. Ann Rev Mar Sci. 4, 63–78. https://doi.org/10.1146/annurev-marine-120710-100926

Grebmeier, JM, Mcroy, CP (1989) Pelagic-benthic coupling on the shelf of the northern Bering and Chukchi Seas. III. Benthic food supply and carbon cycling. Mar Ecol Prog Ser 53, 93–100. https://doi.org/0171-8630/89/0053/0079/$ 03.00

Moran, SB, Ellis, KM, Smith, JN (1997) $^{234}Th/^{238}U$ disequilibrium in the central Arctic Ocean: Implications for particulate organic carbon export. Deep Sea Res II 44, 1593–1606. https://doi.org/10.1016/S0967-0645(97)00049-0

Osborne E, Richter-Menge J, Jeffries M (2018) Arctic Report Card 2018, https://www.arctic.noaa.gov/Report-Card

Piepenburg, D (2005) Recent research on Arctic benthos: Common notions need to be revised. Polar Biol 28, 733–755. https://doi.org/10.1007/s00300-005-0013-5

Pirtle-Levy, R, Grebmeier, JM, Cooper, LW, Larsen, IL (2009) Chlorophyll a in Arctic sediments implies long persistence of algal pigments. Deep Sea Res II 56, 1326–1338. https://doi.org/10.1016/j.dsr2.2008.10.022

Wassmann, P, Reigstad, M (2011) Future Arctic Ocean seasonal ice zones and implications for pelagic-benthic coupling. Oceanography 24, 220–231.